The Cryosphere Discuss., 8, 5539–5588, 2014
www.the-cryosphere-discuss.net/8/5539/2014/
doi:10.5194/tcd-8-5539-2014

The Cryosphere Discussions
Open Access

Simulating the Antarctic ice sheet in the Late-Pliocene warm period: PLISMIP-ANT, an ice-sheet model intercomparison project

B. de Boer[1,2], A. M. Dolan[3], J. Bernales[4,5], E. Gasson[6], H. Goelzer[7], N. R. Golledge[8,9], J. Sutter[10], P. Huybrechts[7], G. Lohmann[10], I. Rogozhina[5], A. Abe-Ouchi[11], F. Saito[12], and R. S. W. van de Wal[2]

[1]Department of Earth Sciences, Faculty of Geosciences, Utrecht University, Utrecht, the Netherlands
[2]Institute for Marine and Atmospheric research Utrecht, Utrecht University, Utrecht, the Netherlands
[3]School of Earth and Environment, University of Leeds, Leeds, UK
[4]Freie Universitaet Berlin, Berlin, Germany
[5]Helmholtz Centre Potsdam, GFZ German Research Centre for Geosciences, Potsdam, Germany
[6]Climate System Research Center, University of Massachusetts Amherst, Amherst, Massachusetts, USA

[7]Earth System Sciences & Departement Geografie, Vrije Universiteit Brussel, Brussels, Belgium
[8]Antarctic Research Centre, Victoria University of Wellington, Wellington, New Zealand
[9]GNS Science, Avalon, 5011 Lower Hutt, New Zealand
[10]Alfred Wegener Institute, Bremerhaven, Germany
[11]Atmosphere and Ocean Research Institute, The University of Tokyo, Kashiwa, 277-8568, Japan
[12]Department of Integrated Climate Change Projection Research, JAMSTEC, Yokohama, Japan

Received: 13 October 2014 – Accepted: 16 October 2014 – Published: 5 November 2014

Correspondence to: B. de Boer (b.deboer@uu.nl)

Published by Copernicus Publications on behalf of the European Geosciences Union.

TCD
8, 5539–5588, 2014

Abstract

In the context of future climate change, understanding the nature and behaviour of ice sheets during warm intervals in Earth history is of fundamental importance. The Late-Pliocene warm period (also known as the PRISM interval: 3.264 to 3.025 million years before present) can serve as a potential analogue for projected future climates. Although Pliocene ice locations and extents are still poorly constrained, a significant contribution to sea-level rise should be expected from both the Greenland ice sheet and the West and East Antarctic ice sheets based on palaeo sea-level reconstructions. Here, we present results from simulations of the Antarctic ice sheet by means of an international Pliocene Ice Sheet Modeling Intercomparison Project (PLISMIP-ANT). For the experiments, ice-sheet models including the shallow ice and shelf approximations have been used to simulate the complete Antarctic domain (including grounded and floating ice). We compare the performance of six existing numerical ice-sheet models in simulating modern control and Pliocene ice sheets by a suite of four sensitivity experiments. Ice-sheet model forcing fields are taken from the HadCM3 atmosphere–ocean climate model runs for the pre-industrial and the Pliocene. We include an overview of the different ice-sheet models used and how specific model configurations influence the resulting Pliocene Antarctic ice sheet. The six ice-sheet models simulate a comparable present-day ice sheet, although the models are setup with their own parameter settings. For the Pliocene simulations using the Bedmap1 bedrock topography, some models show a small retreat of the East Antarctic ice sheet, which is thought to have happened during the Pliocene for the Wilkes and Aurora basins. This can be ascribed to either the surface mass balance, as the HadCM3 Pliocene climate shows a significant increase over the Wilkes and Aurora basin, or the initial bedrock topography. For the latter, our simulations with the recently published Bedmap2 bedrock topography indicate a significantly larger contribution to Pliocene sea-level rise from the East Antarctic ice sheet for all six models relative to the simulations with Bedmap1.

TCD
8, 5539–5588, 2014

1 Introduction

There is uncertainty in the contribution of the Antarctic ice sheet (AIS) to future sea-level change (Church et al., 2013). Projected changes in the surface mass balance (SMB) are shown to be small and are largely estimated to be positive due to an increase in precipitation (Church et al., 2013). However, recent studies show that the oceanic melting and/or calving of the floating parts of the AIS, the ice shelves, is substantial (Pritchard et al., 2012; Rignot et al., 2013), and that an increase in sub-shelf melting can have a significant impact on grounded ice (e.g. Goldberg et al., 2012). Nonetheless, the sensitivity of the AIS to changes in ocean temperatures remains largely uncertain (Church et al., 2013).

Studying past intervals with a warmer than present-day (PD) climate can be used to gain a better understanding of the sensitivity of the AIS to predicted future climate warming. One such warm interval is the Late-Pliocene warm period (also known as the PRISM interval, 3.264 to 3.025 million years before present; Dowsett et al., 2010), which can be considered as a possible analogue for future climate change at the end of this century. During the Late-Pliocene, atmospheric CO_2 concentrations are estimated to vary between 300 and 450 ppm (e.g. Bartoli et al., 2011), although an other estimate (Badger et al., 2013) also indicates lower concentrations close to the interglacial values found in ice cores (Lüthi et al., 2008). This warm period is a well studied interval in Earth's history using both models (e.g. Dolan et al., 2011; Haywood et al., 2013) and data (e.g. Salzmann et al., 2013; Dowsett et al., 2013).

Regardless of the rather large uncertainty of the atmospheric CO_2 concentration during this time period, multiple proxy estimates for temperatures show a clear signal of warming over the globe (Dowsett et al., 2010). In recent years the Pliocene Modelling Intercomparison Project (PlioMIP) has provided a framework for studying the Pliocene with climate models (Haywood et al., 2010, 2011). PlioMIP includes both atmosphere-only and coupled Atmosphere–Ocean General Circulation Models (AOGCMs). CO_2 levels for the PlioMIP experiments were set to 405 ppm (Haywood et al.,

TCD
8, 5539–5588, 2014

2010, 2011) and further boundary conditions are based on the PRISM3 global reconstruction (Dowsett et al., 2010). For PlioMIP eight AO-GCMs were used to study both changes in sea surface and surface–air temperatures during the Late-Pliocene warm period. The models simulated an increase of the global mean surface–air temperature between 1.84 and 3.60 °C compared to the pre-industrial (Haywood et al., 2013). Although the range of the ensemble is quite large, the models appear to be able to reproduce the broad scale features of the Late-Pliocene climate as evidenced in the proxy records (Dowsett et al., 2011, 2013; Haywood et al., 2013; Salzmann et al., 2013).

For the Late-Pliocene warm period, estimates of the change in sea level are in the order of 10–30 m above PD (Raymo et al., 2011; Rovere et al., 2014; Rohling et al., 2014). This requires a significant contribution from the Greenland (Koenig et al., 2014) and the AIS. Large parts of the West Antarctic ice sheet (WAIS) are grounded on bedrock well below sea level (down to ∼ 1500 m). Hence, this ice sheet is more likely to disintegrate when ocean and atmosphere temperatures increase. This is shown by both sediment data (Naish et al., 2009) and modelling studies of the AIS for interglacials throughout the Plio-Pleistocene (Pollard and DeConto, 2009; de Boer et al., 2014). A contribution from the East Antarctic ice sheet (EAIS) may also be expected. However, thus far transient simulations with ice-sheet models have not been capable of reproducing a substantial retreat of the EAIS (Pollard and DeConto, 2012b; de Boer et al., 2014) as has been indicated by marine sediments (Williams et al., 2010; Cook et al., 2013). A few modelling studies did show that the Wilkes and Aurora basins are sensitive to a particular climate forcing (Hill, 2009; Dolan et al., 2011). However, this result was based on an SIA-only ISM.

In this study we investigate the nature and behaviour of the AIS during the Late-Pliocene warm period in terms of the Pliocene Ice Sheet Modelling Intercomparison Project (PLISMIP; Dolan et al., 2012). For this particular study of Antarctica, from now on referred to as PLISMIP-ANT, we use state of the art ice-sheet models (ISMs) that model both grounded and floating ice. Here, we aim to quantify the sea-level contribution from the AIS calculated with different ISMs forced by output of the HadCM3

TCD
8, 5539–5588, 2014

AO-GCM Pliocene experiment (the same as Bragg et al., 2012). We have performed control experiments with pre-industrial and PD climate forcing to evaluate the equilibrium response of each model to the PD climate. Additionally we conducted two experiments forced with Late-Pliocene climate forcing, one initialised with the PD ice sheet, and one that starts with the much smaller Pliocene ice sheet, as used by HadCM3 and PRISM3. The four experiments are summarised in Table 1.

2 Methods

The basic setup of PLISMIP-ANT follows the experimental design outlined in Dolan et al. (2012). All experiments described here are steady state simulations for 100 000 years (100 kyr). We thus focus on the equilibrated response of the ice sheets to a particular climate forcing. Following Dolan et al. (2012) all models use the same climate forcing and same surface-temperature lapse rate correction of $-8\,^{\circ}\mathrm{C\,km^{-1}}$:

$$T_{\mathrm{surf}}(t) = T_{\mathrm{GCM}} - 0.008\,(H_{\mathrm{surf}}(t) - H_{\mathrm{GCM}})\,, \tag{1}$$

with T_{surf} the temperature at the surface of the ice sheet and T_{GCM} the temperature field of the climate model in $^{\circ}$C, H_{surf} the surface elevation of the ice-sheet and H_{GCM} the surface topography of the climate model in m. Here, we firstly describe the experimental design as implemented specifically for PLISMIP-ANT. Secondly, the different climatologies of each experiment are described and compared. Lastly, we specify the setup of the ISMs.

2.1 Experimental design

To force the ISMs over Antarctica we use the monthly climatology obtained from simulations using the Hadley Centre Coupled Atmosphere Ocean Model version 3 (HadCM3; Pope et al., 2000; Gordon et al., 2000), which are set-up following the PlioMIP experimental design (Haywood et al., 2011) and are comparable to those presented in Bragg

TCD
8, 5539–5588, 2014

et al. (2012). The participants use their models to run the ISM over Antarctica including ice shelves. All ISMs are initialised using a suite of boundary conditions. A complete description of PLISMIP within PlioMIP is given by Dolan et al. (2012), however, for PLISMIP-ANT some modifications have been made to the experimental design that we describe here. As shown in Table 1, for PLISMIP-ANT four experiments are performed. In addition to the atmospheric forcing of precipitation and temperature, we also use yearly-averaged ocean temperatures from the ocean model of HadCM3 as input for the ISMs. The main setup of the experiments requires ISMs that are fully capable of simulating both grounded and floating ice, using the approximate stress balance equations for ice sheets; the Shallow Ice Approximation (SIA) and for ice shelves; the Shallow Shelf Approximation (SSA). Additionally, as a sensitivity experiment we also include three SIA-only models that are only capable of simulating grounded ice.

2.2 Model boundary conditions

The model spread between the eight climate models used in PlioMIP is quite substantial (see Fig. 3 in Haywood et al., 2013). However, the different models seem to largely agree that a significant polar amplification has occurred over the Antarctic region. For the current setup of the project we use one AO-GCM climate forcing from PlioMIP (HadCM3). Our choice of HadCM3 as the initial climate model for use in PLISMIP-ANT is based on the long history of usage of HadCM3 within Pliocene climate modelling (e.g. Haywood and Valdes, 2004) and because it is a model with an average climate sensitivity, which simulates average Pliocene temperature changes in relation to predictions from the rest of the PlioMIP ensemble. For the first control experiment, we use a pre-industrial simulation of HadCM3 that includes the PD topography and ice sheets and uses a pCO_2 of 280 ppm. The yearly mean climatology is shown in Fig. 1a–d.

We perform a second control simulation using PD reanalysis of ERA-40 for the surface climatology (Uppala et al., 2005) (Fig. 1e and f) and the World Ocean Database 2009 data set for ocean temperatures (Boyer et al., 2009) as illustrated in Fig. 1h. The climatology of ERA-40 is a bit warmer, averaged over the continent 4 °C and

TCD
8, 5539–5588, 2014

a bit wetter, around 0.2–0.5 m yr^{-1} more precipitation in coastal areas compared to the pre-industrial simulation of HadCM3. However, the largest differences occur over the interior of East Antarctica, where precipitation is up to a factor 5 lower. This has quite a significant influence on the reconstructed ice volume as will be shown later on. Nonetheless, we use of the ERA-40 and the WOD-09 data sets as a secondary control test to simulate the present-day ice sheet and to show the response of the ISMs to different climatologies of the late Holocene.

Both Pliocene simulations are forced with the Pliocene run of HadCM3, which uses the PRISM3 boundary conditions and a pCO_2 of 405 ppm, illustrated in Fig. 1i–l. Here ocean temperatures are depicted at the bottom of the PD ice-shelves of Bedmap1, which are horizontally extrapolated from the nearest ocean grid points since HadCM3 uses a modern land–sea mask, i.e. the alternate experimental design as given by Haywood et al. (2011). Outside the ice shelves sea surface temperatures are shown. Mainly due to the smaller AIS in PRISM3 the surface–air temperatures over Antarctica are warmer by about 7 °C on average compared to the pre-industrial climate. Similarly, the absence of ice in the Wilkes and Aurora basin results in an increase in annual total precipitation of about 0.4–0.6 m yr^{-1} over this particular region. Large temperature differences are also found in the ocean where sub-surface temperatures show a widespread increase of $\sim$ 2.6 °C on average.

For all ISMs we have provided monthly climatology of surface–air temperature and precipitation and yearly mean ocean temperatures at 19 depth levels for HadCM3 and 30 levels from the WOD-09 data set, ranging from the surface to $\sim$ 4.5 km depth. As a lower boundary condition for the 3-D ice-sheet temperature field, the preferred boundary condition is taken to be the heatflux field from Shapiro and Ritzwoller (2004). For the initial ice-sheet thickness and bedrock topography we have used the Bedmap (Bedmap1) data set (Lythe et al., 2001) for the PD configuration and the PRISM3 ice sheet (Dowsett et al., 2010) for the Pliocene. We have also performed the same experiments using the recently published updated bedrock data set of Bedmap2 (Fretwell et al., 2013).

TCD
8, 5539–5588, 2014

All climate fields are projected on a 40 km by 40 km grid, 167 × 167 grid points, using a stereographic projection with OBLIMAP v2.0 (basic theory described in Reerink et al., 2010). For the projection a central longitude was used of 0° E, the central latitude was set to the south pole (i.e. hence in this case a polar stereographic projection) and the angle that defines the standard parallel was set to 24.7° (for details see Reerink et al., 2010). The projection we use here requires a correction for the area of the grid points of the ISMs, for which we follow the methods described in Snyder (1987) with a latitude of true scale of 65.3°. All volumes of the ice sheet and the contribution to sea level are calculated using the corrected area of each grid point.

2.3 Ice-sheet models

For simulating the Antarctic ice sheet over its complete domain in PLISMIP-ANT, we use ISMs that solve both ice flow for grounded and for floating ice. The models in this study include approximate equations of the Stokes equations of flow. The approximations are primarily based on the shallowness of a large ice body, with spatial scales that are much larger than the thickness of the ice. For grounded ice the SIA (Appendix A1; Hutter, 1983) is used. The SIA only considers horizontal shear stresses and assumes the force of gravity to be the main driver of ice flow. On the other hand, for the ice streams and ice shelves, horizontal stretching, or a membrane-type flow is dominant, which is described with the SSA (Appendix A2; Morland, 1987). Both the SIA and SSA use enhancement factors for the flow parameter (see Appendix A). In general velocities are underestimated by the SIA and overestimated by the SSA (Ma et al., 2010). Recent developments in ISMs also include higher-order physics, or the full-Stokes solution of 3-D ice flow (see for example Pattyn et al., 2013). However, for paleoclimate applications that largely investigate the long term, on the order of 10–100 kyr, response of ice sheet, shallow models are still predominantly used (e.g. Huybrechts, 2002; Pollard, 2010; Pollard and DeConto, 2012b; Golledge et al., 2012; de Boer et al., 2014).

All participants were asked to set up the ISM in a standard mode. In other words, use the models at their regular setup with their own parameter settings for the

TCD
8, 5539–5588, 2014

thermodynamics, mass balance and ice flow as would be used for regular paleoclimate simulations. The reasoning behind this is that we get an estimate in the differences in ice volume between different modelling groups that use their normal setups of the models, as they are used for other applications as well. By including the fixed lapse rate correction, Eq. (1), all ISMs are initially forced with the same surface temperatures and precipitation fields from the climate models.

All six ISMs that are used calculate ice-velocities with the SIA and SSA, see Table 3a. Since it would be too exhaustive to describe here all aspects of the different models, we will provide a short description of each model and its specific methodology of calculating ice velocities, the surface mass balance and how the sub-shelf melting is included using the ocean temperatures from the climate forcing. The latter is described below, since this is generally a new aspect in most models. For a more detailed description of each ISM, the reader is referred to their respective references as included at the bottom of Table 3a. All models incorporate a bedrock model, which is adjusted to changes in ice loading. For all models the basic Elastic Lithosphere, Relaxing Asthenosphere (ELRA) model has been used (Le Meur and Huybrechts, 1996).

A new aspect for most of the ISMs used in PLISMIP-ANT is the sub-shelf melting, or basal mass balance, which includes a parameterisation using ocean temperatures as climate forcing. For recent and future mass loss of the AIS, oceanic sub-shelf melting has been found to be significant (Pritchard et al., 2012; Rignot et al., 2013) and as such it is an important component to be included in the total mass budget of the ice sheet, especially for the much warmer ocean temperatures of the Late-Pliocene (see Fig. 1c and k). Most models use a parameterisation as described by Holland and Jenkins (1999) and Beckmann and Goosse (2003):

$$M_{\text{shelf}} = \rho_{\text{w}} c_{p_{\text{O}}} \gamma_{\text{T}} F_{\text{melt}} (T_{\text{oc}} - T_{\text{f}}) / L \rho_{\text{i}}, \quad (2)$$

TCD
8, 5539–5588, 2014

with the different parameters as described in Table 2. T_{oc} is the temperature of the ocean underneath the ice shelf, as vertically interpolated from the 3-D ocean temperature fields from the climate forcing. T_f is the freezing temperature as given by Beckmann and Goosse (2003):

$$T_f = 0.0939 - 0.057 \cdot S_0 + 7.64 \times 10^{-4} z_b, \quad (3)$$

with S_0 a mean value for the salinity of the ocean of 35 psu and z_b the bottom of the ice shelf below sea level. The sub-shelf melt parameter F_{melt} varies between ice-sheet models and is given in Table 3a. Since the HadCM3 climate model does not resolve all points underneath the ice shelves, the ocean temperatures are extrapolated using a distance weighting scheme (similar to Maris et al., 2014).

The SMB is largely calculated using the same method in all models. Precipitation is taken from the climate forcing and from this snow accumulation is determined depending on the surface temperatures. All models except ANICE determine surface melting with a positive degree-day (PDD) scheme (Reeh, 1991), with PDD factors of 8 and 3 mm $(^\circ C\,d)^{-1}$ for ice and snow melt, respectively. Some models additionally include refreezing of rain and melt water.

2.3.1 AISM-VUB

The Antarctic Ice Sheet Model (AISM) from the Vrije Universiteit Brussel (VUB) has been initially developed by Huybrechts (1990, 2002) and was further improved by Fürst (2013) as the version that participated in MISMIP3d (Pattyn et al., 2013). For the present experiments, SIA and SSA are calculated separately for grounded and floating ice and coupled across a one grid-box wide transition zone. Sliding is calculated using a Weertman sliding relation inversely proportional to the height above buoyancy. Surface melting is calculated with the PDD scheme, including meltwater retention by refreezing and capillary forces in the snowpack, driven by the surface temperature field of the climate forcing. Parameter settings are given in Table 3a. Sub-shelf melting is parameterised as a function of local ocean-water temperature above the freezing

TCD
8, 5539–5588, 2014

point using Eq. (1). A distinction is made between protected ice shelves (Ross and Ronne-Filchner) with a melt factor of $F_{melt} = 5.2 \times 10^{-3}\,m\,s^{-1}$ and all other ice shelves with a melt factor of $F_{melt} = 21.8 \times 10^{-3}\,m\,s^{-1}$. The parameters are chosen to reproduce observed average melt rates (Depoorter et al., 2013) under the Ross, Ronne-Filchner and Amery ice shelf for WOD-09 temperature observations and Bedmap2 shelf geometry. For the $Control_{HadCM3}$ run and initial Bedmap1 geometry, average melt rates are a factor 2.0–2.5 too high for these three ice shelves. The two control and the $Pliocene_{Ice\text{-}PRISM3}$ simulations are using an initial spin-up with fixed geometry for 10 kyr and consecutively for 40 kyr with fixed grounding line before the unconstrained 100 kyr simulations. The $Pliocene_{Ice\text{-}PD}$ simulation is integrated forward for 100 kyr restarting from the PD steady state of the $Control_{HadCM3}$ simulation.

2.3.2 ANICE

The ANICE model is part of the IMAU-ICE package (Institute for Marine and Atmospheric research Utrecht), the ice sheet model of Utrecht University. The package contains a range of ISM of different complexities, from shallow 1-D models to a full-stokes application. ANICE calculates both the SIA and SSA velocities for sheet and shelf ice, and add these together. Basal sliding is included as a Mohr–Coulomb plastic law, with basal stresses included in the SSA equations (Winkelmann et al., 2011; de Boer et al., 2013). Surface melting is calculated using an Insolation Temperature Melt (ITM) model, using monthly values of the PD insolation at the top of the atmosphere and surface–air temperature (de Boer et al., 2013). The monthly precipitation field is adjusted with the change in surface temperature, the latter is adjusted according to Eq. (1), Furthermore, refreezing of rain and melt water is calculated using a potential retention fraction. Sub-shelf melting is calculated as described above with the melt factor $F_{melt} = 2 \times 10^{-3}\,m\,s^{-1}$ and is combined with melt rates for exposed ice-shelf and the deep ocean (Pollard and DeConto, 2009; de Boer et al., 2013).

TCD
8, 5539–5588, 2014

2.3.3 PISM

The Parallel Ice Sheet Model (PISM) used for this project is the most recent version v0.6 (Winkelmann et al., 2011; Feldmann et al., 2014). Velocities from the SIA and SSA are combined to yield total velocity (Winkelmann et al., 2011). PISM v0.6 includes a sub-grid scheme described in Feldmann et al. (2014) that improves grounding line migration. Basal sliding is included as a Mohr–Coulomb plastic law, with basal stresses included in the SSA equations (Winkelmann et al., 2011). An elevation-dependent prescription of the till friction angle is used (see Martin et al., 2011), ranging from 6° for all areas of bedrock below 100 m elevation and linearly increasing to 15° for all areas where the bed is above 1500 m elevation. Additionally, the subglacial till layer is also weakened by saturation of meltwater generated at the ice-sheet bed by geothermal, frictional and strain heating (Golledge et al., 2014). Variability in modelled ice volume in the PISM simulations arises from a thermodynamic feedback in which increased basal sliding (leading to volume loss) is the threshold response to a gradual saturation from meltwater saturation of the basal substrate layer. Under a constant climate forcing, these glaciological feedbacks give rise to an ice-sheet that is in a Surface melting is calculated with the PDD scheme. The sub-shelf melting rates are calculated with a modified form of the quadratic parameterisation of Holland et al. (2008):

$$M_{\text{shelf}} = \left(0.341T_{\text{oc}}^2 + 2.365T_{\text{oc}} + 3.003\right)/100. \quad (4)$$

Here, T_{oc} is used at a fixed depth of 600 m, as this was considered most representative of the water depth affecting most of the PD ice shelves. Additionally, two calving criteria are used: firstly, the eigen calving approach of Levermann et al. (2012) that predicts calving losses according to horizontal spreading rates, and secondly a thickness limitation is imposed, such that shelves thinner than 250 m are automatically calved. The latter is a tuned value found through experimentation to yield ice shelf extents of reasonable fit to observed geometries.

TCD
8, 5539–5588, 2014

2.3.4 PSU-ISM

The Penn State University (PSU) ISM has been widely used for paleoclimate applications (e.g. Pollard and DeConto, 2009, 2012a, b). The most recent version includes a grounding-line flux boundary condition as introduced by Schoof (2007), whereas a heuristic scheme is used to determine the transition from sheet to shelf ice flow (Pollard and DeConto, 2012b). Sliding is included as the standard Weertman sliding, but the basal sliding coefficients were tuned to minimise modern-day ice surface elevation errors (Pollard and DeConto, 2012b). The tuned coefficients are adopted from Pollard and DeConto (2012b), the tuning is not repeated in this study. Surface melting is included using a basic PDD scheme. The sub-shelf melt rates use the same Eq. (2), but with a quadratic function of $(T_{oc} - T_f)$, following (Holland et al., 2008), and an additional melt factor $K = 3$ (see Pollard and DeConto, 2012b, Eq. 17) with $F_{melt} = 5 \times 10^{-3}\,m\,s^{-1}$.

2.3.5 RIMBAY

RIMBAY is based on the 3-D ISM by Pattyn (2003) and a full description is given in Thoma et al. (2014). RIMBAY combines SIA and SSA velocities in a similar way as PISM and ANICE. in RIMBAY the SSA and SIA velocities are added together with a smoothing gradient over the grounding line (Thoma et al., 2014), which mixes SIA and SSA velocities over 2 grid boxes, i.e. a distance of 80 km, to smooth the transition between SIA and SSA regions. Sliding is included with a basic Weertman sliding law. Surface melting is calculated with a PDD scheme. Sub-shelf melting is calculated as described above with the melt factor $F_{melt} = 11 \times 10^{-3}\,m\,s^{-1}$.

2.3.6 SICOPOLIS

Here we use SICOPOLIS (SImulation COde for POLythermal Ice Sheets) version 3.2-dev revision 498. The model calculates the SIA and SSA separately for sheet and shelf flow, respectively. The enhancement factor for ice flow on land are separate for glacial

TCD
8, 5539–5588, 2014

and interglacial ice. $E_{SIA} = 5$ for glacial ice (older than 11 kyr for the Control simulations) and $E_{SIA} = 1$ for interglacial ice, consistent with measurements from ice cores (NEEM community members, 2013). No additional grounding line or combinations are used. Sliding is calculated with a Weertman type sliding law (Sato and Greve, 2012). Surface melting is calculated with the PDD scheme, supplemented by the semi-analytical solution for the PDD integral by Calov and Greve (2005). Further, the model implements a retention model that takes into account the contribution from rainfall and surface melt to the formation of superimposed ice, for which a saturation factor of 0.6 is chosen (Reeh, 1991). The sub-shelf melting parametrisation is as described above, with different melt factors, $F_{melt} = 5 \times 10^{-3}\,m\,s^{-1}$ for protected, $F_{melt} = 5 \times 10^{-2}\,m\,s^{-1}$ for exposed and $F_{melt} = 5 \times 10^{-1}\,m\,s^{-1}$ for open ocean shelves. Additionally, melting at the grounding line points is included using the regression of Rignot and Jacobs (2002).

3 Results

All experiments are 100 kyr steady state runs, i.e. a constant climate forces the ISMs, for which only surface temperatures are adjusted with a constant lapse rate, Eq. (1), and ocean temperatures are adjusted according with the depth of the bottom of the shelves. Figure 2 shows the full 100 kyr simulated ice volume of all models for all four experiments of PLISMIP-ANT. The model behaviour varies considerably due to differences in specifying initial conditions between the models, i.e. initial ice temperatures and differences in calculating velocities and the surface mass balance. In general, the models do come into an equilibrium state quite rapidly.

3.1 Modern control simulations of Antarctica

For PLISMIP-ANT two control simulations have been performed. The first simulation is the basic test for a comparison with the Pliocene HadCM3 forcing and uses a pre-industrial simulation of HadCM3 (Fig. 1a–d). Differences in the time-evolution of

TCD
8, 5539–5588, 2014

the models can be mainly ascribed to the initial ice-temperature distribution and consequently velocities of the ice (Fig. 2a). Most ISMs displays the strongest increase in ice volume at the beginning of the 100 kyr simulation. However, the variability thereafter is quite limited, whereas some models, such as the PSU-ISM (green), show a smaller initial increase in ice volume and a steady increase of volume during the 100 kyr simulation. The different initial ice volume of AISM is caused by the initialisation procedure performed before the equilibrated 100 kyr run (see Sect. 2.3.1). Variability in ice volume in the PISM simulations arises from a thermodynamic feedback in which increased basal sliding (leading to volume loss) is the threshold response to a gradual saturation from meltwater saturation of the basal substrate layer. Under a constant climate forcing, these glaciological feedbacks give rise to an ice-sheet that is in a state of dynamic equilibrium (Van Pelt and Oerlemans, 2012; Golledge et al., 2014).

In general, the final ice volume between models differs quite substantially, 25.96 to 29.59 $\times 10^6$ km^3 for the Control$_{\text{HadCM3}}$ simulation relative to the 26.55 $\times 10^6$ km^3 for the Bedmap1 PD grounded ice volume (Fig. 4). Nonetheless, the topography and the extent of the ice shelves are rather similar compared to the PD initial ice sheet (Fig. 3). Although the setup of the ISMs is different, the difference of the final topography of the ISMs compared to the observed Bedmap1 surface elevation shows a rather similar pattern, i.e. a lower topography in the interior of the ice sheet and thicker ice around the edges, especially in the Lambert ice shelf, the Antarctic Peninsula and Coats land (see Fig. S1 in the Supplement). The decrease in ice thickness in the centre and the growth on the edges is a common feature in shallow ice-sheet models and can be ascribed to the course spatial resolution that does not capture the detailed topography and unknown basal conditions (e.g. Martin et al., 2011; Maris et al., 2014; Briggs et al., 2014).

The Control$_{\text{Obs}}$ simulation with ERA-40 and WOD-09 climate forcing in general shows a smaller ice sheet compared to the pre-industrial control with HadCM3, with a range of 24.11 to 26.86 $\times 10^6$ km^3 as illustrated in Fig. 4. The lower ice thickness in the interior of the EAIS is mainly due to lower precipitation over this area, which is

TCD
8, 5539–5588, 2014

known to be underestimated in ERA-40 and models of present-day climatology (Van de Berg et al., 2005). Most ISMs do reconstruct an ice sheet that remains comparable to the PD ice volume and extent (Fig. S2). The extent of the ice shelves is simulated less well by particularly PISM and SICOPOLIS, which is due to lower ice velocities across the grounding line and a lower SMB over the ice-shelves areas.

When comparing the two control experiments (Fig. 4), AISM simulates ice sheets that are both larger than PD, whereas SICOPOLIS simulates ice sheets smaller than PD, the latter with a smaller extent of grounded ice, mainly due to locally too high rates of grounding line melting. RIMBAY and ANICE simulate ice volume closest to the PD, but ANICE shows a smaller ice extent. The largest difference between the two control simulations is shown by PISM and the PSU-ISM (Fig. 4), which could attributed to the difference in SMB over grounded ice, and the lowest ice fluxes across the grounding line, relative to the other models.

3.2 Antarctica in the Late-Pliocene

As shown in Table 1, we have performed two Pliocene experiments with the same HadCM3 climate forcing. Pliocene$_{\text{Ice-PD}}$ simulation uses the PD ice sheet as an initial state for the ISMs, whereas the Pliocene$_{\text{Ice-PRISM3}}$ simulation is initialised with the much smaller PRISM3 ice sheet topography. For both simulations the response over the 100 kyr simulations is very different for the ISMs (Fig. 2c and d). For the Pliocene$_{\text{Ice-PD}}$ experiment the AISM, PSU-ISM and RIMBAY show an increase in ice volume, whereas ANICE, PISM and SICOPOLIS show a much smaller final ice sheet (Fig. 2c). The three models with a smaller ice sheet behave in a similar way in the Pliocene$_{\text{Ice-PRISM3}}$ simulation, as shown in Fig. 2d.

The final ice-sheet topographies are shown in Fig. 5. The warmer ocean temperatures in the Late-Pliocene climate forcing (see Fig. 1k compared to Fig. 1c) result in complete disintegration of the ice shelves from the PD initial ice sheet for all models except RIMBAY (Fig. 5i). For all six ISMs the ice sheet has a larger volume in the Pliocene$_{\text{Ice-PD}}$ simulations compared to the Pliocene$_{\text{Ice-PRISM3}}$ simulation (Fig. 6a).

TCD
8, 5539–5588, 2014

Moreover, when considering East and West Antarctica independently (Fig. S3), there are some interesting features within the PLISMIP-ANT ensemble. Volume predictions for East Antarctica vary from 22.04 to 25.45 × 10^6 km^3 using the PD as an initial condition and from 21.01 to 24.08 × 10^6 km^3 using the PRISM3 ice sheet to initialise the ISMs. When starting with a smaller ice sheet, three models simulate a reduction in EAIS volume in comparison to modern (PISM, RIMBAY and SICOPOLIS). Nevertheless, none of the models sustain the extent of retreat prescribed in PRISM3 (Figs. 5 and 6c). Furthermore, the largest difference between the two Pliocene simulations for the WAIS (see Fig. S3b) is simulated by RIMBAY, 1.79 to 6.42 × 10^6 km^3 and by the PSU-ISM 1.95 to 3.98 × 10^6 km^3.

3.3 Intercomparison

Figure 7 provides an overview of the results from all four experiments in terms of ice sheet thickness. On a grid-box by grid-box basis, the ensemble of results has been sorted into order of thickness (thinnest to thickest members) and we have plotted the median (i.e. the mean of the 3rd and 4th member; Fig. 7 – left panels) and the range (i.e. the difference between the largest and smallest ice thickness, divided by two; Fig. 7 – middle panels). Finally, we have also plotted ice sheet presence which shows how many of the six ISMs predict ice of any thickness in that particular grid box. The ice presence maps (Fig. 7 – right panels) show that all models reconstruct an EAIS of near-modern extent for the Late-Pliocene, and that no ISM simulates the retreat in the Wilkes and Aurora basin as prescribed by the PRISM3 boundary conditions.

The range of ice thickness in model predictions illustrates the degree of model agreement among the PLISMIP-ANT ensemble. The differences among the models are large, in particular for the $Pliocene_{Ice\text{-}PD}$ simulation (Fig. 7h). In addition (Fig. 7i) shows where some models suggest a large-scale ice cover across West Antarctica and others only small ice caps. For the $Pliocene_{Ice\text{-}PRISM3}$ simulation, initialised with the PRISM3 ice sheet, the median shows a smaller WAIS, whereas the EAIS is similar to that of the $Pliocene_{Ice\text{-}PD}$ simulation (Fig. 7j). Most models do simulate ice on the

TCD
8, 5539–5588, 2014

West Antarctic land areas but no ISM shows a vast increase of the WAIS, which is prohibited by the warm ocean temperatures (Fig. 1k). The largest range in thickness for the $\text{Pliocene}_{\text{Ice-PRISM3}}$ experiment is exhibited over the Wilkes and Aurora basin in East Antarctica (Fig. 7k). All ISMs simulate an advance over this area of the ice sheet relative to the initial PRISM3 ice-sheet topography (Fig. 7l), the large range is largely due to differences in SMB and ice velocities.

In Fig. 8 we show cross sections through the ice sheets resulting from the six ISMs for three locations. The cross sections are shown in Fig. 7a and represent the regions with the largest spread among the models. Figure 8a and b show the cross sections through the Wilkes basin (A in Fig. 7a), for the $\text{Control}_{\text{HadCM3}}$ and $\text{Pliocene}_{\text{Ice-PD}}$ simulations respectively. For the $\text{Control}_{\text{HadCM3}}$ simulation (In Fig. 8a) the modelled topographies are largely similar, whereas the spread between the ISMs for the $\text{Pliocene}_{\text{Ice-PD}}$ simulation (In Fig. 8b) is notably larger. For the Lambert ice stream (B in Fig. 7a) the spread among the ISM simulations is large for all four experiments. All models generally show thicker ice for the $\text{Control}_{\text{HadCM3}}$ simulation relative to PD (see also Fig. S1), whereas for the $\text{Pliocene}_{\text{Ice-PD}}$ the ice thicknesses vary but cluster around the initial PRISM3 surface elevation (In Fig. 8d). Similar for the Lambert ice stream, all ISMs simulate a higher topography over the cross-sectional area of the WAIS (Fig. 8e). As can be seen in Fig. 7h, the spread between the models is particularly large over West Antarctica for the $\text{Pliocene}_{\text{Ice-PD}}$ simulation, with some models simulating a large ice sheet and others predicting ice-free conditions (Fig. 8f).

3.4 Sensitivity to initial bedrock topography

Recently, a new data set of bedrock topography, surface elevation and ice thickness for Antarctica (Bedmap2, Fretwell et al., 2013) has been published. To analyse the sensitivity of the modelled ice-sheet geometry to the new bedrock topography inferred from observations we have repeated the same experiments with the Bedmap2 data set, using exactly the same setup as was used for the original experiments. The Bedmap2 data set provides a significant improvement relative to the Bedmap1 data set used

TCD
8, 5539–5588, 2014

here, i.e. higher resolution, improved data coverage and precision (Fretwell et al., 2013). Moreover, Bedmap2 contains fewer inconsistencies between surface elevation, ice thickness and bedrock topography, which was a limitation in the Bedmap1 data set (Fretwell et al., 2013).

To repeat the experiments, a new initial Pliocene ice sheet topography had to be generated for the Pliocene$_{\text{Ice-PRISM3}}$ simulation. Here we have placed the PRISM3 ice-sheet configuration on the Bedmap2 bedrock topography. To account for the uplift of the bed due to the retreat of the ice sheet, relative to the Bedmap2 ice thickness, the ELRA bedrock model has been used to run the bedrock topography to isostatic equilibrium. The final bedrock topography and ice-sheet surface are then used as initial fields for the Pliocene$_{\text{Ice-PRISM3}}$ experiment as shown in Fig. 9a. In general, differences with the original PRISM3 ice sheet are not large. However, bedrock elevation is significantly lower in the Wilkes and Aurora basin (see Fig. 9h). Naturally, some uncertainties are involved in this procedure such as the chosen bedrock model and its parameters and the accompanying uncertainties in the Bedmap2 data set (see Figs. 11 and 12 in Fretwell et al., 2013). However, we believe this is a reasonable first sensitivity test to identify how the ISMs respond to a different initial bedrock topography.

As is shown in Fig. 9, the final simulated surface topography shows a different result especially for the Wilkes and Aurora basin, where observations have improved considerably. The smaller ice sheets for the Pliocene$_{\text{Ice-PRISM3}}$ simulation result in a reduced ice volume. As shown in Fig. S4a, most models calculate an even lower volume than the initial PRISM3 ice sheet, also due to a reduced size of the central part of the ice sheet, whereas the area covered by ice is still larger (see Fig. S4c). Four out of the six ISMs simulate a final ice volume for the Pliocene$_{\text{Ice-PRISM3}}$ experiment that is lower than the initial PRISM3 ice volume (21.24×10^6 km^3 for Bedmap2 relative to 21.04×10^6 km^3 for Bedmap1). Figure 10 present a comparison between the two simulations. The Bedmap2 simulations for Control$_{\text{HadCM3}}$ are also comparable to the PD ice-sheet extent and ice volume. Final ice volume for the Pliocene$_{\text{Ice-PRISM3}}$ experiment

TCD
8, 5539–5588, 2014

is 19.72 to 24.37 × 10^6 km^3 for Bedmap2 compared to 22.70 to 25.95 × 10^6 km^3 for the simulation using the Bedmap1 data set.

4 Discussion

For the control simulations, all ISMs reconstruct an ice sheet close to its PD configuration and result in a smaller equilibrated ice sheet driven by the ERA-40/WOD-09 climate (Fig. 4), mainly due to the drier conditions across East Antarctica in ERA-40 relative to the pre-industrial simulation of HadCM3. The differences between the models for all four experiments are rather small considering that all models are used with their own setup for determining ice temperatures and velocities. Differences between model is largely due to the variability in ice fluxes, whereas the average SMB for the six ISMs is 2113.3 ± 129.7 $Gt\,yr^{-1}$ (Gt = 10^{12} kg) and the ice flux across the grounding line is 346.5 ± 147.8 $Gt\,yr^{-1}$ at the final step of each 100 kyr simulation.

Most ISMs for the two Pliocene simulations have a similar final steady-state topography (Figs. 5 and 6) and show a retreat of the WAIS from its PD configuration in the Pliocene$_{\text{Ice-PD}}$ simulation due to the higher ocean temperatures which enhance sub-shelf melting. Only RIMBAY simulates a WAIS that is larger than PD (Fig. S3) and the PSU-ISM simulates a rather large WAIS as well, although the ice shelves have completely disintegrated. For the EAIS all models produce a similar final surface topography and final volume for the two simulations. Here most ISMs do show an increase in ice volume for the Pliocene$_{\text{Ice-PD}}$ simulation relative to PD, mainly caused by a higher accumulation in the Wilkes and Aurora basins relative to the pre-industrial (see Fig. 1j). The largest difference is found in the simulations by RIMBAY. Although surface–air and ocean temperatures are largely the same at the initial step of each 100 kyr simulation of each ISM, model simulations show quite a strong divergence for the two Pliocene simulations (Fig. 2c and d). The divergent behaviour within our intercomparison is largely due to differences in ice fluxes and sub-shelf melting (not shown), i.e. two features in the models that are not constrained in our experimental setup.

TCD
8, 5539–5588, 2014

4.1 Comparison with SIA-only ISMs

The initial setup of PLISMIP was comprised of models that include the SIA only (Dolan et al., 2012), similar to the experiments performed for Greenland (Koenig et al., 2014). Although a combination of the SIA and SSA is necessary to simulate the complete domain of the AIS, the main driver of ice flow for the EAIS is the SIA-based ice flow velocity. Here, we compare simulations with three SIA ISMs to the modelled EAIS with the SIA-SSA models. The three models are IcIES (Saito and Abe-Ouchi, 2004), BASISM (Hindmarsh, 2001) and IMAU-ICE, a SIA version of ANICE (de Boer et al., 2013). All three models use the SIA as described in Appendix A1 and use a Weertman type sliding law and have been used for the Greenland experiments as well, as described in Koenig et al. (2014). IMAU-ICE is largely similar to ANICE, only uses Weertman sliding.

As is shown in Fig. S3c, final ice volume for the EAIS falls within the range of the SIA-SSA models, with IcIES on the low end and BASISM on the high end of the spectrum of SIA-SSA models. Similar to the six SIA-SSA models with Bedmap2, the three SIA-only models all show a smaller ice extent over the Wilkes and Aurora basins (Fig. 9i–k). Also, all three models simulate a smaller ice volume using Bedmap2 (Fig. S4b and d) relative to Bedmap1 (Fig. 6b and d). SIA-only models could be used for modelling the East Antarctic ice sheet, but to capture the interaction with the ocean, SSA ice-shelf dynamics are essential for the long-term transient behaviour of Antarctica.

4.2 Contribution to Late-Pliocene sea level

The contribution of Antarctica to sea level during the Late-Pliocene is shown in Table 4. All values are derived from the total ice volume at the last time step of each 100 kyr simulation relative to the PD mapped ice sheet on the 40 by 40 km grid, using ice thickness above flotation and a correction for bedrock change:

TCD
8, 5539–5588, 2014

$$\Delta S = \left(\sum_{i,j} \mathrm{Hi}_{0af} - \mathrm{Hi}_{af} + \min(0, \mathrm{Hb}) - \min(0, \mathrm{Hb}_0) \right) \times 40\,000 \times 40\,000 / O_{\mathrm{area}}. \quad (5)$$

where Hi_{0af} and Hi_{af} are the ice thickness above flotation for the initial (either Bedmap1 or Bedmap2) and final modelled ice sheet in m water equivalent, respectively:

$$\mathrm{Hi}_{af} = \frac{\rho_i}{\rho_w} \mathrm{Hi} + \mathrm{Hb}. \quad (6)$$

Density of ice and seawater are taken as provided in Table 2 and an ocean area is used of $O_{\mathrm{area}} = 3.62 \times 10^{14} \mathrm{m}^2$. Hb is the bedrock topography (in m; negative below sea level). Although the spread is quite considerable, all ISMs simulate a higher sea level for the $\mathrm{Pliocene}_{\mathrm{Ice\text{-}PRISM3}}$ simulation relative to the $\mathrm{Control}_{\mathrm{HadCM3}}$ simulation, average value of 7.57 ± 2.99 m s.e. (1 standard deviation) for the Bedmap1 simulations and 9.76 ± 2.13 m s.e. for the simulations with Bedmap2. For the Bedmap1 simulations, the relative contribution of most models is largely due to a too large ice sheet for the $\mathrm{Control}_{\mathrm{HadCM3}}$ simulation (Fig. 10a). On average, the six ISMs calculate a sea-level contribution of -3.23 ± 2.93 m s.e. for the $\mathrm{Control}_{\mathrm{HadCM3}}$ simulation relative to Bedmap1. Especially for AISM and PSU-ISM, this is a significant bias since their modelled $\mathrm{Pliocene}_{\mathrm{Ice\text{-}PRISM3}}$ sea-level contribution is rather small (Table 4). On the contrary, for the Bedmap2 simulations on average the ISMs produce a too small ice sheet of only 1.11 ± 3.02 m s.e. for the $\mathrm{Control}_{\mathrm{HadCM3}}$ simulation. Hence, the bias is smaller and the contribution to Pliocene sea-level rise can be considered more significant, although uncertainties remain.

5 Conclusions

The results presented here are the first steady state simulations of the full domain of the AIS, using coupled SIA-SSA ISMs for the Pliocene Ice Sheet Modelling Intercomparison Project, PLISMIP. Firstly, the control simulations show a consistent result for

TCD
8, 5539–5588, 2014

all ISMs, all models simulate a lower ice volume for the PD ERA-40/WOD-09 data set compared to the simulation with HadCM3 pre-industrial climatology due to a drier East Antarctic climate in ERA-40. Secondly, for the Pliocene simulations using the Bedmap1 bedrock topography and ice thickness, all models show a consistent result with a higher final ice volume of the $\text{Pliocene}_{\text{Ice-PD}}$ simulation compared to that of the simulation initialised with the PRISM3 ice sheet. RIMBAY shows the largest difference between the $\text{Pliocene}_{\text{Ice-PD}}$ simulation and the $\text{Pliocene}_{\text{Ice-PRISM3}}$ simulation. All six ISMs were used in their regular setup. Hence, the calculation of thermodynamics (thus ice fluxes) and the sub-shelf melting (see Sect. 2.3 and Table 3a) was done different for each ISM. Surface–air and ocean temperatures have initially the same values for each model, but differences in final ice volumes calculated by the ISMs can be largely ascribed to differences in ice fluxes and sub-shelf melting.

Our simulations of the Late-Pliocene warm period with Bedmap1 do not show a retreat of the EAIS from the Wilkes and Aurora basins as has been suggested by studies of marine sediments (e.g. Williams et al., 2010; Cook et al., 2013). Thus far transient simulations through the Late-Pliocene were not capable of simulating a significant retreat either (Pollard and DeConto, 2012b; de Boer et al., 2014). On the other hand, the experiments using the Bedmap2 initial ice sheet do suggest that an additional contribution from the EAIS should be considered likely. Our simulations indicate significantly less ice over the Wilkes and Aurora basins and a more considerable and less biased contribution to Pliocene sea level relative to the simulations with Bedmap1. These sensitivity experiments show the importance of including an accurate data set of bedrock topography for ice sheet models, which is in line with Mengel and Levermann (2014). Additionally, a future study in which we aim to incorporate climate fields from different AO-GCMs (Haywood et al., 2013) will allow evaluation of the uncertainties in climate forcing on the steady state response of the modelled AIS. For the Greenland ice sheet a previous intercomparison showed that this is important to take into account (Dolan et al., 2014). The spread in surface–air and ocean temperatures between AO-GCMs over Antarctica is considerable (Haywood et al., 2013) and it is likely that both

TCD
8, 5539–5588, 2014

calculated SMB and sub-shelf melting will contribute to a large spread in the modelled AIS sea-level contribution.

Appendix A: Approximations in ice-sheet modelling

All ISMs used within PLISMIP-ANT apply the shallow ice and shallow shelf (or shelfy stream) approximations to reduce computational time relative to solving the full Stokes equations of flow. Here we shortly describe the two approximations.

A1 The Shallow Ice Approximation (SIA)

For modelling 3-D ice sheets over long time scales, the SIA is commonly used to calculate ice flow over land areas (e.g. Hutter, 1983; Huybrechts, 1990). For the SIA the normal, longitudinal, stresses are neglected relative to the horizontal shear stress. In this way, shearing stresses induced by vertical changes of the horizontal velocities are only balanced by the driving stress: $\rho_i g H \nabla H_s$. The SIA velocities follow from an integral equation:

$$\boldsymbol{V}_{\mathrm{SIA}} = -2(\rho_i g)^n |\nabla H_s|^{n-1} \nabla H_s \int_b^z E_{\mathrm{SIA}} A(T^*)(H_s - z)^n \mathrm{d}\zeta. \quad \text{(A1)}$$

Here, ∇H_s is the horizontal surface slope, ζ the scaled vertical coordinate, $\rho_i = 910\,\mathrm{kg\,m^{-3}}$ the density of ice, $g = 9.81\,\mathrm{m\,s^{-2}}$ the gravity acceleration and $n = 3$ the flow exponent in Glen's flow law. $A(T^*)$ is the flow-rate factor ($\mathrm{Pa^{-3}\,yr^{-1}}$) depending on the ice temperature corrected for pressure melting dependent (T^*). E_{SIA} is the flow enhancement factor (Ma et al., 2010), which is different for each ISM (see Table 3a).

TCD
8, 5539–5588, 2014

A2 The Shallow Shelf Approximation (SSA)

To determine ice velocities for ice shelves, the approximate stress balance for the SSA includes longitudinal stress which are more dominant compared to the shear stress. The balance equations determine stretching velocities, i.e. the change of the horizontal velocities independent of depth in the horizontal plane. The SSA is largely used to calculate the velocities of ice shelves and ice streams (e.g. Morland, 1987; Bueler and Brown, 2009). For the latter basal friction needs to be included:

$$\frac{\partial}{\partial x}\left[2\mu H_{\mathrm{i}}\left(2\frac{\partial u}{\partial x}+\frac{\partial v}{\partial y}\right)\right]+\frac{\partial}{\partial y}\left[\mu H_{\mathrm{i}}\left(\frac{\partial u}{\partial y}+\frac{\partial v}{\partial x}\right)\right](+\tau_{\mathrm{b},x})=\rho g H_{\mathrm{i}}\frac{\partial H_{\mathrm{s}}}{\partial x}, \tag{A2}$$

$$\frac{\partial}{\partial y}\left[2\mu H_{\mathrm{i}}\left(2\frac{\partial v}{\partial y}+\frac{\partial u}{\partial x}\right)\right]+\frac{\partial}{\partial x}\left[\mu H_{\mathrm{i}}\left(\frac{\partial v}{\partial x}+\frac{\partial u}{\partial y}\right)\right](+\tau_{\mathrm{b},y})=\rho g H_{\mathrm{i}}\frac{\partial H_{\mathrm{s}}}{\partial y}. \tag{A3}$$

Here, u and v are the SSA velocities in the x and y direction, respectively (in $\mathrm{m\,yr^{-1}}$) and H_{i} is the ice thickness. For the SSA the stresses due to stretching are balanced by the gravitational driving stress and possibly the basal stresses $\tau_{\mathrm{b},x}$ and $\tau_{\mathrm{b},y}$ (in Pa) when applied on land. The parameter μ is the vertical averaged viscosity, a function of the strain rates and the vertical mean flow rate factor $A(T^*)$ (e.g. Bueler and Brown, 2009):

$$\mu=\frac{1}{2(E_{\mathrm{SSA}}\overline{A})^{1/n}}\left[\left(\frac{\partial u}{\partial x}\right)^2+\left(\frac{\partial v}{\partial y}\right)^2+\left(\frac{\partial u}{\partial x}\right)\left(\frac{\partial v}{\partial y}\right)+\frac{1}{4}\left(\frac{\partial u}{\partial y}+\frac{\partial v}{\partial x}\right)^2\right]^{\frac{1-n}{2n}}, \tag{A4}$$

with $\overline{A}$ the vertical mean flow rate factor $A(T^*)$ and E_{SSA} the enhancement factor for the SSA velocities (Ma et al., 2010), which is different for each ISM (see Table 3a).

The Supplement related to this article is available online at doi:10.5194/tcd-8-5539-2014-supplement.

TCD
8, 5539–5588, 2014

Acknowledgements. Financial support for B. d. Boer was provided through the NWO-VICI grant of L. J. Lourens. A. M. Dolan acknowledges funding from the European Research Council under the European Union's Seventh Framework Programme (FP7/2007-2013)/ERC grant agreement no. 278636. E. Gasson supported by PLIOMAX, US National Science Foundation award OCE-1202632. ANICE model runs were performed on the LISA Computer Cluster, B. d. Boer would like to acknowledge SurfSARA Computing and Networking Services for their support. HadCM3 simulations were performed at the University of Leeds.

References

Badger, M. P. S., Schmidt, D. N., Mackensen, A., and Pancost, R. D.: High-resolution alkenone palaeobarometry indicates relatively stable pCO_2 during the Pliocene (3.3–2.8 Ma), Philos. T. Roy. Soc. A, 371, 20130094, doi:10.1098/rsta.2013.0094, 2013. 5542

Bartoli, G., Hönisch, B., and Zeebe, R. E.: Atmospheric CO_2 decline during the Pliocene intensification of Northern Hemisphere glaciations, Paleoceanography, 26, PA4213, doi:10.1029/2010PA002055, 2011. 5542

Beckmann, A. and Goosse, H.: A parameterization of ice shelf-ocean interaction for climate models, Ocean Model., 5, 157–170, 2003. 5548, 5549, 5576

Boyer, T. P., Antonov, J. I., Baranova, O. K., Garcia, H. E., Johnson, D. R., Locarnini, R. A., Mishonov, A. V., O'Brien, T. D., Seidov, D., Smolyar, I. V., and Zweng, M. M.: World Ocean Database 2009, in: NOAA Atlas NESDIS 66, edited by: Levitus, S., US Gov. Printing Office, Washington, D.C., 216 pp., 2009. 5545, 5579

Bragg, F. J., Lunt, D. J., and Haywood, A. M.: Mid-Pliocene climate modelled using the UK Hadley Centre Model: PlioMIP Experiments 1 and 2, Geosci. Model Dev., 5, 1109–1125, doi:10.5194/gmd-5-1109-2012, 2012. 5544

Briggs, R. D., Pollard, D., and Tarasov, L.: A data-constrained large ensemble analysis of Antarctic evolution since the Eemian, Quaternary Sci. Rev., 103, 91–115, 2014. 5554

Bueler, E. and Brown, J.: Shallow shelf approximation as a "sliding law" in a thermomechanically coupled ice sheet model, J. Geophys. Res., 114, F03008, doi:10.1029/2008JF001179, 2009. 5564

Calov, R. and Greve, R.: Correspondence. A semi-analytical solution for the positive degree-day model with stochastic temperature variations, J. Glaciol., 51, 173–175, 2005. 5553

TCD
8, 5539–5588, 2014

Church, J., Clark, P., Cazenave, A., Gregory, J., Jevrejeva, S., Levermann, A., Merrifield, M., Milne, G., Nerem, R., Nunn, P., Payne, A., Pfeffer, W., Stammer, D., and Unnikrishnan, A.: Sea level change, in: Climate Change 2013: The Physical Science Basis, Contribution of Working Group I to the Fifth Assessment Report of the Intergovernmental Panel on Climate Change, edited by: Stocker, T., Qin, D., Plattner, G.-K., Tignor, M., Allen, S., Boschung, J., Nauels, A., Xia, Y., Bex, V., and Midgle, P., Cambridge University Press, Cambridge, UK and New York, NY, USA, 1137–1216, 2013. 5542

Cook, C. P., van de Flierdt, T., Williams, T., Hemming, S. R., Iwai, M., Kobayashi, M., Jimenez-Espejo, F. J., Escutia, C., Gonzalez, J. J., Khim, B.-K., McKay, R. M., Passchier, S., Bohaty, S. M., Riesselman, C. R., Tauxe, L., Sugisaki, S., Galindo, A. L., Patterson, M. O., Sangiorgi, F., Pierce, E. L., Brinkhuis, H., Klaus, A., Fehr, A., Bendle, J. A. P., Bijl, P. K., Carr, S. A., Dunbar, R. B., Flores, J. A., Hayden, T. G., Katsuki, K., Kong, G. S., Nakai, M., Olney, M. P., Pekar, S. F., Pross, J., Rohl, U., Sakai, T., Shrivastava, P. K., Stickley, C. E., Tuo, S., Welsh, K., and Yamane, M.: Dynamic behaviour of the East Antarctic ice sheet during Pliocene warmth, Nat. Geosci., 6, 765–769, 2013. 5543, 5562

de Boer, B., van de Wal, R. S. W., Lourens, L. J., and Bintanja, R.: A continuous simulation of global ice volume over the past 1 million years with 3-D ice-sheet models, Clim. Dynam., 41, 1365–1384, 2013. 5550, 5560, 5576

de Boer, B., Lourens, L. J., and van de Wal, R. S. W.: Persistent 400,000 year variability of Antarctic ice volume and the carbon-cycle is revealed throughout the Plio-Pleistocene, Nat. Commun., 5, 2999, doi:10.1038/ncomms3999, 2014. 5543, 5547, 5562

Depoorter, M. A., Bamber, J. L., Griggs, J. A., Lenaerts, J. T. M., Ligtenberg, S. R. M., van den Broeke, M. R., and Moholdt, G.: Calving fluxes and basal melt rates of Antarctic ice shelves, Nature, 502, 89–92, 2013. 5550

Dolan, A. M., Haywood, A. M., Hill, D. J., Dowsett, H. J., Hunter, S. J., Lunt, D. J., and Pickering, S. J.: Sensitivity of Pliocene ice sheets to orbital forcing, Palaeogeogr. Palaeocl., 309, 98–110, 2011. 5542, 5543

Dolan, A. M., Koenig, S. J., Hill, D. J., Haywood, A. M., and DeConto, R. M.: Pliocene Ice Sheet Modelling Intercomparison Project (PLISMIP) – experimental design, Geosci. Model Dev., 5, 963–974, doi:10.5194/gmd-5-963-2012, 2012. 5543, 5544, 5545, 5560, 5574

TCD
8, 5539–5588, 2014

Dolan, A. M., Hunter, S. J., Hill, D. J., Haywood, A. M., Koenig, S. J., Otto-Bliesner, B. L., Abe-Ouchi, A., Bragg, F., Chan, W.-L., Chandler, M. A., Contoux, C., Jost, A., Kamae, Y., Lohmann, G., Lunt, D. J., Ramstein, G., Rosenbloom, N. A., Sohl, L., Stepanek, C., Ueda, H., Yan, Q., and Zhang, Z.: Using results from the PlioMIP ensemble to investigate the Greenland Ice Sheet during the warm Pliocene, Clim. Past Discuss., 10, 3483–3535, doi:10.5194/cpd-10-3483-2014, 2014. 5562

Dowsett, H. J., Robinson, M., Haywood, A. M., Hill, D. J., Sohl, L. E., Chandler, M. A., Williams, M., Foley, K., and Stoll, D.: The PRISM3D paleoenvironmental reconstruction, Stratigraphy, 7, 123–139, 2010. 5542, 5543, 5546, 5574

Dowsett, H. J., Haywood, A. M., Valdes, P. J., Robinson, M. M., Lunt, D. J., Hill, D. J., Stoll, D. K., and Foley, K. M.: Sea surface temperatures of the mid-PiacenzianWarm period: a comparison of PRISM3 and HadCM3, Palaeogeogr. Palaeocl., 309, 83–91, 2011. 5543

Dowsett, H. J., Foley, K. M., Stoll, D. K., Chandler, M. A., Sohl, L. E., Bentsen, M., Otto-Bliesner, B. L., Bragg, F. J., Chan, W.-L., Contoux, C., Dolan, A. M., Haywood, A. M., Jonas, J. A., Jost, A., Kamae, Y., Lohmann, G., Lunt, D. J., Nisancioglu, K. H., Abe-Ouchi, A., Ramstein, G., Riesselman, C. R., Robinson, M. M., Rosenbloom, N. A., Salzmann, U., Stepanek, C., Strother, S. L., Ueda, H., Yan, Q., and Zhang, Z.: Sea Surface Temperature of the mid-Piacenzian Ocean: a Data-Model Comparison, Sci. Rep. 3, doi:10.1038/srep02013, 2013. 5542, 5543

Feldmann, J., Albrecht, T., Khroulev, C., Pattyn, F., and Levermann, A.: Resolution-dependent performance of grounding line motion in a shallow model compared with a full-Stokes model according to the MISMIP3d intercomparison, J. Glaciol., 60, 353–360, 2014. 5551

Fretwell, P., Pritchard, H. D., Vaughan, D. G., Bamber, J. L., Barrand, N. E., Bell, R., Bianchi, C., Bingham, R. G., Blankenship, D. D., Casassa, G., Catania, G., Callens, D., Conway, H., Cook, A. J., Corr, H. F. J., Damaske, D., Damm, V., Ferraccioli, F., Forsberg, R., Fujita, S., Gim, Y., Gogineni, P., Griggs, J. A., Hindmarsh, R. C. A., Holmlund, P., Holt, J. W., Jacobel, R. W., Jenkins, A., Jokat, W., Jordan, T., King, E. C., Kohler, J., Krabill, W., Riger-Kusk, M., Langley, K. A., Leitchenkov, G., Leuschen, C., Luyendyk, B. P., Matsuoka, K., Mouginot, J., Nitsche, F. O., Nogi, Y., Nost, O. A., Popov, S. V., Rignot, E., Rippin, D. M., Rivera, A., Roberts, J., Ross, N., Siegert, M. J., Smith, A. M., Steinhage, D., Studinger, M., Sun, B., Tinto, B. K., Welch, B. C., Wilson, D., Young, D. A., Xiangbin, C., and Zirizzotti, A.: Bedmap2: improved ice bed, surface and thickness datasets for Antarctica, The Cryosphere, 7, 375–393, doi:10.5194/tc-7-375-2013, 2013. 5546, 5557, 5558

TCD
8, 5539–5588, 2014

Fürst, J.: Dynamic response of the Greenland ice sheet to future climatic warming, Ph.D. thesis, Vrije Universiteit Brussel, Brussel, 2013. 5549, 5576

Goldberg, D. N., Little, C. M., Sergienko, O. V., Gnanadesikan, A., Hallberg, R., and Oppenheimer, M.: Investigation of land ice–ocean interaction with a fully coupled ice–ocean model: 2. Sensitivity to external forcings, J. Geophys. Res., 117, F02038, doi:10.1029/2011JF002247, 2012. 5542

Golledge, N. R., Fogwill, C. J., Mackintosh, A. N., and Buckley, K. M.: Dynamics of the last glacial maximum Antarctic ice-sheet and its response to ocean forcing, P. Natl. Acad. Sci. USA, 109, 16052–16056, 2012. 5547, 5576

Golledge, N. R., Menviel, L., Carter, L., Fogwill, C. J., England, M. H., Cortese, G., and Levy, R. H.: Antarctic contribution to meltwater pulse 1A from reduced Southern Ocean overturning, Nat. Commun., 5, 5107, doi:10.1038/ncomms6107, 2014. 5551, 5554

Gordon, C., Cooper, C., Senior, C. A., Banks, H., Gregory, J. M., Johns, T. C., Mitchell, J. F. B., and Wood, R. A.: The simulation of SST, sea ice extents and ocean heat transports in a version of the Hadley Centre coupled model without flux adjustments, Clim. Dynam., 16, 147–168, 2000. 5544

Haywood, A. M. and Valdes, P.: Modelling Pliocene warmth: contribution of atmosphere, oceans and cryosphere, Earth Planet. Sc. Lett., 218, 363–377, 2004. 5545

Haywood, A. M., Dowsett, H. J., Otto-Bliesner, B., Chandler, M. A., Dolan, A. M., Hill, D. J., Lunt, D. J., Robinson, M. M., Rosenbloom, N., Salzmann, U., and Sohl, L. E.: Pliocene Model Intercomparison Project (PlioMIP): experimental design and boundary conditions (Experiment 1), Geosci. Model Dev., 3, 227–242, doi:10.5194/gmd-3-227-2010, 2010. 5542

Haywood, A. M., Dowsett, H. J., Robinson, M. M., Stoll, D. K., Dolan, A. M., Lunt, D. J., Otto-Bliesner, B., and Chandler, M. A.: Pliocene Model Intercomparison Project (PlioMIP): experimental design and boundary conditions (Experiment 2), Geosci. Model Dev., 4, 571–577, doi:10.5194/gmd-4-571-2011, 2011. 5542, 5543, 5544, 5546, 5579

Haywood, A. M., Hill, D. J., Dolan, A. M., Otto-Bliesner, B. L., Bragg, F., Chan, W.-L., Chandler, M. A., Contoux, C., Dowsett, H. J., Jost, A., Kamae, Y., Lohmann, G., Lunt, D. J., Abe-Ouchi, A., Pickering, S. J., Ramstein, G., Rosenbloom, N. A., Salzmann, U., Sohl, L., Stepanek, C., Ueda, H., Yan, Q., and Zhang, Z.: Large-scale features of Pliocene climate: results from the Pliocene Model Intercomparison Project, Clim. Past, 9, 191–209, doi:10.5194/cp-9-191-2013, 2013. 5542, 5543, 5545, 5562

TCD
8, 5539–5588, 2014

Hill, D. J.: Modelling Earth's Cryosphere during peak Pliocene warmth, Ph.D. Thesis, University of Bristol, Bristol, 2009. 5543
Hindmarsh, R. C. A.: Influence of channelling on heating in ice-sheet flows, Geophys. Res. Lett., 28, 3681–3684, 2001. 5560
Holland, D. and Jenkins, A.: Modeling thermodynamic ice–ocean interactions at the base of an ice shelf, J. Phys. Oceanogr., 29, 1787–1800, 1999. 5548
Holland, P. R., Jenkins, A., and Holland, D. M.: The response of ice shelf basal melting to variations in ocean temperature, J. Climate, 21, 2558–2572, 2008. 5551, 5552, 5576
Hutter, K.: Theoretical Glaciology, D. Reidel, Dordrecht, 1983. 5547, 5563
Huybrechts, P.: A 3-D model for the Antarctic ice sheet: a sensitivity study on the glacial–interglacial contrast, Clim. Dynam., 5, 79–92, 1990. 5549, 5563, 5576
Huybrechts, P.: Sea-level changes at the LGM from ice-dynamic reconstructions of the Greenland and Antarctic ice sheets during the glacial cycles, Quaternary Sci. Rev., 21, 203–231, 2002. 5547, 5549, 5576
Koenig, S. J., Dolan, A. M., de Boer, B., Stone, E. J., Hill, D. J., DeConto, R. M., Abe-Ouchi, A., Lunt, D. J., Pollard, D., Quiquet, A., Saito, F., Savage, J., and van de Wal, R.: Greenland Ice Sheet sensitivity and sea level contribution in the mid-Pliocene warm period – Pliocene Ice Sheet Model Intercomparison Project PLISMIP, Clim. Past Discuss., 10, 2821–2856, doi:10.5194/cpd-10-2821-2014, 2014. 5543, 5560
Le Meur, E. and Huybrechts, P.: A comparision of different ways of dealing with isostacy: examples from modelling the Antarctic ice sheet during the last glacial cycle, Ann. Glaciol., 23, 309–317, 1996. 5548
Levermann, A., Albrecht, T., Winkelmann, R., Martin, M. A., Haseloff, M., and Joughin, I.: Kinematic first-order calving law implies potential for abrupt ice-shelf retreat, The Cryosphere, 6, 273–286, doi:10.5194/tc-6-273-2012, 2012. 5551
Lüthi, D., Le Flock, M., Bereiter, B., Blunier, T., Barnola, J.-M., Siegenthaler, U., Raynaud, D., Jouzel, J., Fischer, H., Kawamura, K., and Stocker, T.: High-resolution carbon dioxide concentration record 650 000–800 000 years before present, Nature, 453, 379–382, 2008. 5542
Lythe, M. B., Vaughan, D. G., and the BEDMAP Consortium: BEDMAP: a new ice thickness and subglacial topographic model of Antarctica, J. Geophys. Res., 106, 11335–11351, doi:10.1029/2000JB900449, 2001. 5546, 5574

TCD
8, 5539–5588, 2014

Ma, Y., Gagliardini, O., Ritz, C., Gillet-Chaulet, F., Durand, G., and Montagnat, M.: Enhancement factors for grounded ice and ice shelves inferred from an anisotropic ice-flow model, J. Glaciol., 56, 805–812, 2010. 5547, 5563, 5564

Maris, M. N. A., de Boer, B., Ligtenberg, S. R. M., Crucifix, M., van de Berg, W. J., and Oerlemans, J.: Modelling the evolution of the Antarctic ice sheet since the last interglacial, The Cryosphere, 8, 1347–1360, doi:10.5194/tc-8-1347-2014, 2014. 5549, 5554

Martin, M. A., Winkelmann, R., Haseloff, M., Albrecht, T., Bueler, E., Khroulev, C., and Levermann, A.: The Potsdam Parallel Ice Sheet Model (PISM-PIK) – Part 2: Dynamic equilibrium simulation of the Antarctic ice sheet, The Cryosphere, 5, 727–740, doi:10.5194/tc-5-727-2011, 2011. 5551, 5554

Mengel, M. and Levermann, A.: Ice plug prevents irreversible discharge from East Antarctica, Nature Clim. Change, 4, 451–455, 2014. 5562

Morland, L. W.: Unconfined ice-shelf flow, in: Dynamics of the West Antarctic Ice Sheet, edited by: de Veen, C. J. V. and Oerlemans, J., D. Reidel, Dordrecht, 99–116, 1987. 5547, 5564

Naish, T., Powell, R., Levy, R., Wilson, G., Scherer, R., Talarico, F., Krissek, L., Niessen, F., Pompilio, M., Wilson, T., Carter, L., DeConto, R., Huybers, P., McKay, R., Pollard, D., Ross, J., Winter, D., Barrett, P., Browne, G., Cody, R., Cowan, E., Crampton, J., Dunbar, G., Dunbar, N., Florindo, F., Gebhardt, C., Graham, I., Hannah, M., Hansaraj, D., Harwood, D., Helling, D., Henrys, S., Hinnov, L., Kuhn, G., Kyle, P., Laufer, A., Maffioli, P., Magens, D., Mandernack, K., McIntosh, W., Millan, C., Morin, R., Ohneiser, C., Paulsen, T., Persico, D., Raine, I., Reed, J., Riesselman, C., Sagnotti, L., Schmitt, D., Sjunneskog, C., Strong, P., Taviani, M., Vogel, S., Wilch, T., and Williams, T.: Obliquity-paced Pliocene West Antarctic ice sheet oscillations, Nature, 458, 322–328, 2009. 5543

NEEM community members: Eemian interglacial reconstructed from a Greenland folded ice core, Nature, 493, 489–494, 2013. 5553

Pattyn, F.: A new three-dimensional higher-order thermomechanical ice sheet model: basic sensitivity, ice stream development, and ice flow across subglacial lakes, J. Geophys. Res., 108, 2382, doi:10.1029/2002JB002329, 2003. 5552

TCD
8, 5539–5588, 2014

Pattyn, F., Perichon, L., Durand, G., Favier, L., Gagliardini, O., Hindmarsh, R. C., Zwinger, T., Albrecht, T., Cornford, S., Docquier, D., Fürst, J. J., Goldberg, D., Gudmundsson, G. H., Humbert, A., Hütten, M., Huybrechts, P., Jouvet, G., Kleiner, T., Larour, E., Martin, D., Morlighem, M., Payne, A. J., Pollard, D., Rückamp, M., Rybak, O., Seroussi, H., Thoma, M., and Wilkens, N.: Grounding-line migration in plan-view marine ice-sheet models: results of the ice2sea MISMIP3d intercomparison, J. Glaciol., 59, 410–422, 2013. 5547, 5549

Pollard, D.: A retrospective look at coupled ice sheet–climate modeling, Climatic Change, 100, 173–194, 2010. 5547

Pollard, D. and DeConto, R. M.: Modelling West Antarctic ice sheet growth and collapse through the past five million years, Nature, 458, 329–332, 2009. 5543, 5550, 5552

Pollard, D. and DeConto, R. M.: A simple inverse method for the distribution of basal sliding coefficients under ice sheets, applied to Antarctica, The Cryosphere, 6, 953–971, doi:10.5194/tc-6-953-2012, 2012a. 5552, 5577

Pollard, D. and DeConto, R. M.: Description of a hybrid ice sheet-shelf model, and application to Antarctica, Geosci. Model Dev., 5, 1273–1295, doi:10.5194/gmd-5-1273-2012, 2012b. 5543, 5547, 5552, 5562, 5577

Pope, V. D., Gallani, M. L., Rowntree, P. R., and Stratton, R. A.: The impact of new physical parametrizations in the Hadley Centre climate model: HadAM3, Clim. Dynam., 16, 123–146, 2000. 5544

Pritchard, H. D., Ligtenberg, S. R. M., Fricker, H. A., Vaughan, D. G., van den Broeke, M. R., and Padman, L.: Antarctic ice-sheet loss driven by basal melting of ice shelves, Nature, 484, 502–505, 2012. 5542, 5548

Raymo, M. E., Mitrovica, J. X., O'Leary, M. J., DeConto, R. M., and Hearty, P. J.: Departures from eustasy in Pliocene sea-level records, Nat. Geosci., 4, 328–332, 2011. 5543

Reeh, N.: Paramterization of melt rate and surface temperature on the Greenland ice-sheet, Polarforschung, 59, 113–128, 1991. 5549, 5553

Reerink, T. J., Kliphuis, M. A., and van de Wal, R. S. W.: Mapping technique of climate fields between GCM's and ice models, Geosci. Model Dev., 3, 13–41, doi:10.5194/gmd-3-13-2010, 2010. 5547

Rignot, E. and Jacobs, S. S.: Rapid bottom melting widespread near Antarctic ice sheet grounding lines, Science, 296, 2020–2023, 2002. 5553

Rignot, E., Jacobs, S., Mouginot, J., and Scheuchl, B.: Ice-shelf melting around Antarctica, Science, 341, 266–270, 2013. 5542, 5548

TCD
8, 5539–5588, 2014

Rohling, E. J., Foster, G. L., Grant, K. M., Marino, G., Roberts, A. P., Tamisiea, M. E., and Williams, F.: Sea-level and deep-sea-temperature variability over the past 5.3 million years, Nature, 508, 477–482, 2014. 5543

Rovere, A., Raymo, M. E., Mitrovica, J. X., Hearty, P. J., O'Leary, M. J., and Inglis, J. D.: The Mid-Pliocene sea-level conundrum: glacial isostasy, eustasy and dynamic topography, Earth Planet. Sc. Lett., 387, 27–33, 2014. 5543

Saito, F. and Abe-Ouchi, A.: Thermal structure of Dome Fuji and east Dronning Maud Land, Antarctica, simulated by a three-dimensional ice-sheet model, Ann. Glaciol., 39, 433–438, 2004. 5560

Salzmann, U., Dolan, A. M., Haywood, A. M., Chan, W.-L., Voss, J., Hill, D. J., Abe-Ouchi, A., Otto-Bliesner, B., Bragg, F. J., Chandler, M. A., Contoux, C., Dowsett, H. J., Jost, A., Kamae, Y., Lohmann, G., Lunt, D. J., Pickering, S. J., Pound, M. J., Ramstein, G., Rosenbloom, N. A., Sohl, L., Stepanek, C., Ueda, H., and Zhang, Z.: Challenges in quantifying Pliocene terrestrial warming revealed by data-model discord, Nat. Clim. Change, 3, 969–974, 2013. 5542, 5543

Sato, T. and Greve, R.: Sensitivity experiments for the Antarctic ice sheet with varied sub-ice-shelf melting rates, Ann. Glaciol., 53, 221–228, 2012. 5553, 5577

Schoof, C.: Ice sheet grounding line dynamics: steady states, stability, and hysteresis, J. Geophys. Res., 112, F03S28, doi:10.1029/2006JF000664, 2007. 5552, 5577

Shapiro, N. M. and Ritzwoller, M. H.: Inferring surface heat flux distribution guided by a global seismic model: particular application to Antarctica, Earth Planet. Sc. Lett., 223, 213–223, 2004. 5546, 5576

Snyder, J. P.: Map projections – a working manual, USGS Professional Paper 1395, available at: http://pubs.er.usgs.gov/usgspubs/pp/pp1395 (last access: November 2014), 1987. 5547

Thoma, M., Grosfeld, K., Barbi, D., Determann, J., Goeller, S., Mayer, C., and Pattyn, F.: RIMBAY – a multi-approximation 3D ice-dynamics model for comprehensive applications: model description and examples, Geosci. Model Dev., 7, 1–21, doi:10.5194/gmd-7-1-2014, 2014. 5552, 5577

TCD
8, 5539–5588, 2014

Uppala, S., Kållberg, P., Simmons, A., Andrae, U., da Costa Bechtold, V., Fiorino, M., Gibson, J., Haseler, J., Hernandez, A., Kelly, G., Li, X., Onogi, K., Saarinen, S., Sokka, N., Allan, R., Andersson, E., Arpe, K., Balmaseda, M., Beljaars, A., van de Berg, L., Bidlot, J., Bormann, N., Caires, S., Chevallier, F., Dethof, A., Dragosavac, M., Fisher, M., Fuentes, M., Hagemann, S., Hólm, E., Hoskins, B., Isaksen, L., Janssen, P., Jenne, R., McNally, A., Mahfouf, J.-F., Morcrette, J.-J., Rayner, N., Saunders, R., Simon, P., Sterl, A., Trenberth, K., Untch, A., Vasiljevic, D., Viterbo, P., and Woollen, J.: The ERA-40 re-analysis, Q. J. Roy. Meteorol. Soc., 131, 2961–3012, 2005. 5545, 5579

Van de Berg, W. J., Van den Broek, M. R., Reijmer, C. H., and Van Meijgeaard, E.: Characteristics of the Antarctic surface mass balance, 1958–2002, using a regional atmospheric climate model, Ann. Glaciol., 41, 97–104, 2005. 5555

Van Pelt, W. J. J. and Oerlemans, J.: Numerical simulations of cyclic behaviour in the Parallel Ice Sheet Model (PISM), J. Glaciol., 58, 347–360, 2012. 5554

Williams, T., van de Flierdt, T., Hemming, S. R., Chung, E., Roy, M., and Goldstein, S. L.: Evidence for iceberg armadas from East Antarctica in the Southern Ocean during the late Miocene and early Pliocene, Earth Planet. Sc. Lett., 290, 351–361, 2010. 5543, 5562

Winkelmann, R., Martin, M. A., Haseloff, M., Albrecht, T., Bueler, E., Khroulev, C., and Levermann, A.: The Potsdam Parallel Ice Sheet Model (PISM-PIK) – Part 1: Model description, The Cryosphere, 5, 715–726, doi:10.5194/tc-5-715-2011, 2011. 5550, 5551, 5576

TCD
8, 5539–5588, 2014

Table 1. Experiments for PLISMIP-ANT following Dolan et al. (2012). Two phases are carried out, a control phase and Pliocene phase. Forcing climatologies for $\text{Control}_{\text{HadCM3}}$ and the Pliocene experiments are taken from an AO-GCM, $\text{Control}_{\text{Obs}}$ uses ERA-40 reanalysis and ocean temperatures from WOD-09. Initial ice sheets are taken from Bedmap (Lythe et al., 2001) and PRISM3 (Dowsett et al., 2010). BC: Boundary Conditions.

Phase	Climate input	Initial ice sheet
$\text{Control}_{\text{HadCM3}}$	Pre-Industrial AO-GCM	Bedmap
$\text{Control}_{\text{Obs}}$	ERA-40 and WOD-09	Bedmap
$\text{Pliocene}_{\text{Ice-PD}}$	Pliocene GCM + PRISM3 BC	Bedmap
$\text{Pliocene}_{\text{Ice-PRISM3}}$	Pliocene GCM + PRISM3 BC	PRISM3

TCD
8, 5539–5588, 2014

Table 2. Physical parameters for the sub-shelf melt parameterisation.

Constant and description		value
ρ_i	ice density ($kg\,m^{-3}$)	910
ρ_w	seawater density ($kg\,m^{-3}$)	1028
c_{p_o}	specific heat capacity of ocean ($J\,kg^{-1}\,°C^{-1}$)	3974
γ_T	thermal exchange velocity ($m\,s^{-1}$)	10^{-4}
L	Latent heat of fusion ($J\,kg^{-1}$)	3.35×10^5

TCD
8, 5539–5588, 2014

Table 3a. Description of the ice-sheet models used for PLISMIP-ANT. All models apply the climatological forcing of temperature and precipitation with absolute values. Models are run on a 40 km by 40 km grid. For the bottom boundary condition of the ice temperature the heat flux field of Shapiro and Ritzwoller (2004) was used. The surface temperature is corrected with a surface lapse-rate of $-8\,^{\circ}\mathrm{C\,km^{-1}}$. SMB: Surface Mass Balance, fd: finite difference, SIA: Shallow Ice Approximation, SSA: Shallow Shelf Approximation, PDD: Positive Degree Day, ITM: Insolation-Temperature Melt, BG03: Beckmann and Goosse (2003).

Charac-teristics	Model name AISM-VUB	ANICE	PISM
Numerical methods	3-D thermo-mechanic, fd SIA, SSA	3-D thermo-mechanic, fd SIA + SSA for floating ice and sliding velocity	3-D thermo-mechanic, fd SIA + SSA for floating ice and sliding velocity
Enh. factors	$E_{SIA} = 2$, $E_{SSA} = 0.9$	$E_{SIA} = 5$, $E_{SSA} = 1$	$E_{SIA} = 2.85$, $E_{SSA} = 0.7$
Time step	1 yr for SMB and Hi 20 yr for Ti and Hb	Adaptive, about 0.5–2 yr for SIA and Hi, 1 month for SMB, 5 yr for SSA and temperature	Adaptive, about 1–20 yr for Hi, SIA and temperature
SMB	PDD + refreezing, PDD factors: $8\,\mathrm{mm\,(^{\circ}C\,d)^{-1}}$ for ice melt $3\,\mathrm{mm\,(^{\circ}C\,d)^{-1}}$ for snow melt	ITM model + refreezing GCM precipitation field is adjusted as function of temp.	PDD $8\,\mathrm{mm\,(^{\circ}C\,d)^{-1}}$ for ice melt $3\,\mathrm{mm\,(^{\circ}C\,d)^{-1}}$ for snow melt
Shelf-melting	BG03 heat flux as function of T_o, vertically interpolated to ice-shelf bottom $F_{melt} = 5.2 \times 10^{-3}\,\mathrm{m\,s^{-1}}$ for protected and $21.8 \times 10^{-3}\,\mathrm{m\,s^{-1}}$ for exposed shelves	BG03 heat flux as function of T_o, vertically interpolated to ice-shelf bottom $F_{melt} = 2 \times 10^{-3}\,\mathrm{m\,s^{-1}}$, plus exposed shelf melt of $3\,\mathrm{m\,yr^{-1}}$ and open ocean melt rate of $5\,\mathrm{m\,yr^{-1}}$	Quadratic relationship from Holland et al. (2008) with T_{oc} at 600 m depth
Basal Sliding	Weertman sliding	Mohr–Coulomb plastic law with basal stress included in SSA	Mohr–Coulomb plastic law with basal stress included in SSA
Referen-ces	Huybrechts (1990, 2002) Fürst (2013)	de Boer et al. (2013)	Golledge et al. (2012) Winkelmann et al. (2011)

TCD
8, 5539–5588, 2014

Table 3b. Continued.

Characteristics	Model name PSU-ISM	RIMBAY	SICOPOLIS
Numerical methods	3-D thermo-mechanic, fd SIA + SSA with grounding line flux boundary condition of Schoof (2007)	3-D thermo-mechanic, fd SIA, SSA	3-D thermo-mechanic, fd SIA, SSA
Enh. factors	$E_{SIA} = 1$, $E_{SSA} = 0.3$	$E_{SIA} = 1$, $E_{SSA} = 1$	$E_{SIA} = 1$ for interglacial ice and
Time step	Adaptive, 2–5 yr for Hi and calving, 50 yr for Ti and Hb 50–100 yr for SMB	3 years for Hi, velocities and temperature	1 year for SIA, SSA and Hi, 5 yr for water content, age and temperature
SMB	PDD 8 mm (°C d)$^{-1}$ for ice melt 3 mm (°C d)$^{-1}$ for snow melt	PDD 8 mm (°C d)$^{-1}$ for ice melt 3 mm (°C d)$^{-1}$ for snow melt	PDD + refreezing, PDD factors: 8 mm (°C d)$^{-1}$ for ice melt 3 mm (°C d)$^{-1}$ for snow melt
Shelf-melting	BG03 heat flux with quadratic function of T_{oc}, vertically interpolated $F_{melt} = 5 \times 10^{-3}$ m s^{-1} with additional factor $K = 3$	BG03 heat flux as function of T_{oc}, vertically interpolated to ice-shelf bottom $F_{melt} = 11 \times 10^{-3}$ m s^{-1}	BG03 heat flux as function of T_o, vertically interpolated to ice-shelf bottom $F_{melt} = 5 \times 10^{-3}$ m s^{-1} for protected, 5×10^{-2} m s^{-1} for exposed and 5×10^{-1} m s^{-1} for open ocean shelves
Basal Sliding	Weertman sliding sliding coefficient tuned	Weertman sliding	Weertman sliding with sub-melt sliding
References	Pollard and DeConto (2012a) Pollard and DeConto (2012b)	Thoma et al. (2014)	Sato and Greve (2012)

TCD
8, 5539–5588, 2014

Table 4. Contribution to the mean sea level (m) for all simulations relative to the initial PD ice sheet using Bedmap1. Contributions are calculated with a constant ocean area of $3.62 \times 10^{14} m^2$ using only grounded ice above flotation and corrected for changed in bedrock elevation. The last columns shows the sea-level contribution of the $Pliocene_{Ice\text{-}PRISM3}$ relative to $Control_{HadCM3}$ simulations of each ISM for Bedmap1 (B1) and Bedmap2 (B2).

ISM	$Ctrl_{HadCM3}$	$Ctrl_{Obs}$	$Pliocene_{Ice\text{-}PD}$	$Pliocene_{Ice\text{-}PRISM3}$	ΔS_{B1}	ΔS_{B2}
AISM	−4.91	−1.06	−3.44	0.25	**5.16**	**8.42**
ANICE	−2.85	1.79	0.54	6.04	**8.89**	**7.66**
PISM	−5.12	2.38	3.00	8.02	**13.14**	**9.71**
PSU-ISM	−7.26	−0.46	−7.97	0.35	**7.61**	**7.96**
RIMBAY	−0.80	2.08	−12.61	6.06	**6.86**	**11.04**
SICOPOLIS	1.54	6.08	0.82	5.29	**3.75**	**13.78**

TCD
8, 5539–5588, 2014

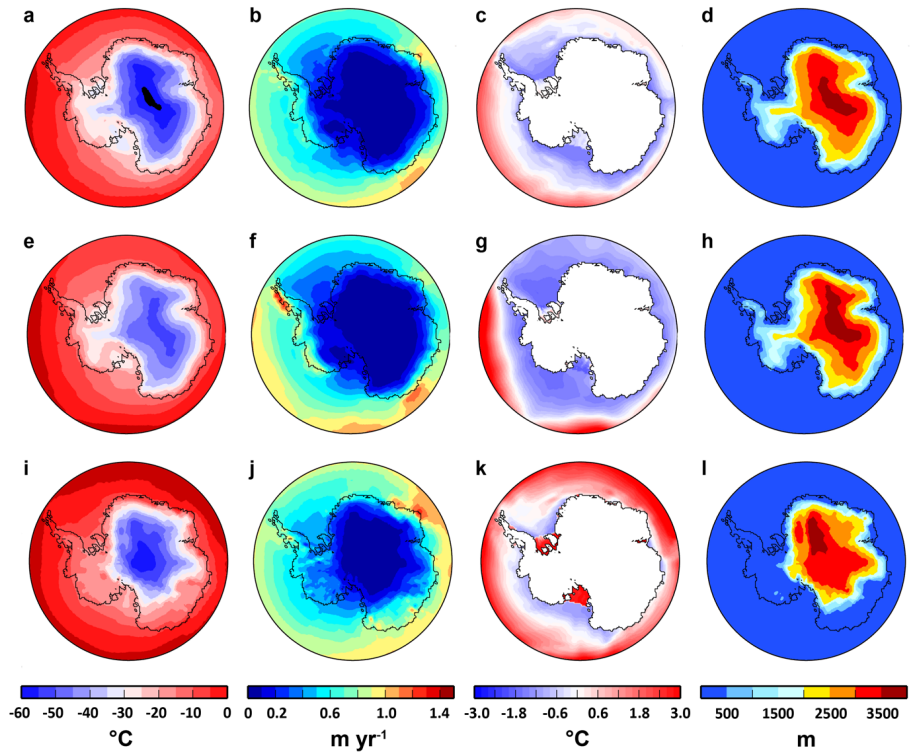

Figure 1. Yearly mean climatology of the three different climate forcing used (see Table 1). Top panels shows results from a pre-industrial run of HadCM3. Middle panels is ERA-40 (1971–2000 reanalysis) (Uppala et al., 2005) and ocean temperatures from the WOD-09 data set (Boyer et al., 2009). Bottom panels illustrate the Pliocene HadCM3 run with full PRISM3 boundary conditions (Haywood et al., 2011). From left to right, surface–air temperature in ˚C, Precipitation in m yr^{-1} water equivalent, sea surface temperatures and temperatures at the bottom of the PD ice shelves in ˚C and surface topography in the climate model in m. The black line in all panels represents the Bedmap1 outline of the grounding line.

TCD
8, 5539–5588, 2014

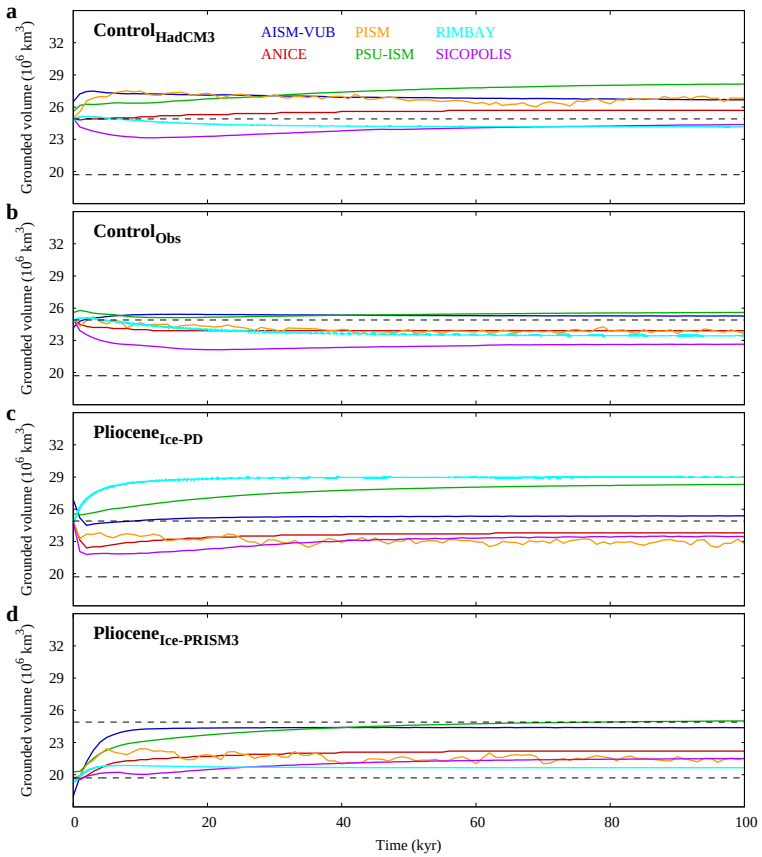

Figure 2. Modelled grounded ice volume over 100 kyr. **(a)** The Control$_{HadCM3}$ simulation, with HadCM3 pre-industrial climate forcing. **(b)** The Control$_{Obs}$ simulation, with ERA-40/WOD09 climate forcing. **(c)** The Pliocene$_{Ice-PD}$ simulation, with HadCM3 Pliocene climate forcing and an initial PD ice sheet. **(d)** The Pliocene$_{Ice-PRISM3}$ simulation, with HadCM3 Pliocene climate forcing and the initial PRISM3 ice sheet.

TCD
8, 5539–5588, 2014

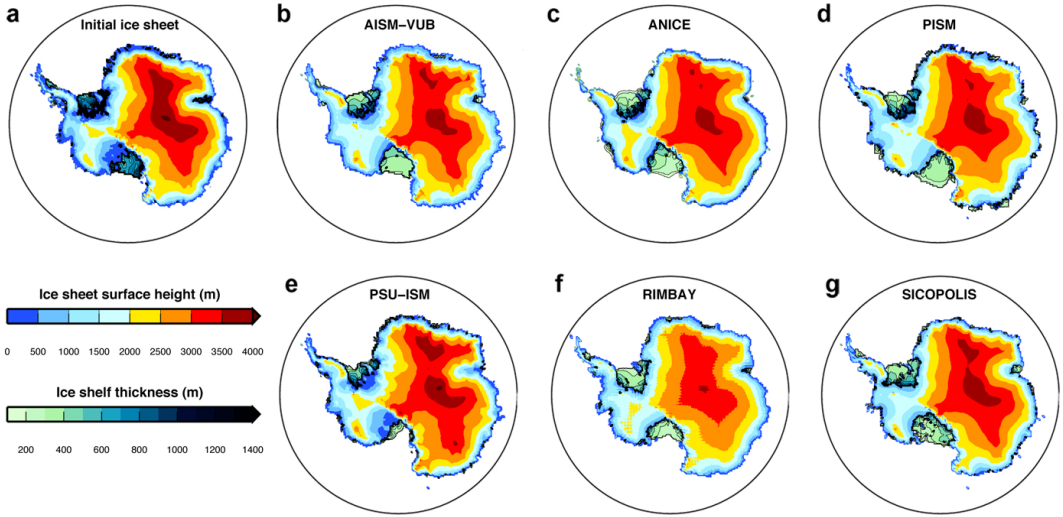

Figure 3. Ice surface topography and thickness of the ice shelves for the $\text{Control}_{\text{HadCM3}}$ simulation, with HadCM3 climate forcing. **(a)** Initial ice sheet, **(b)** AISM, **(c)** ANICE, **(d)** PISM, **(e)** PSU-ISM, **(f)** RIMBAY, **(g)** SICOPOLIS.

TCD
8, 5539–5588, 2014

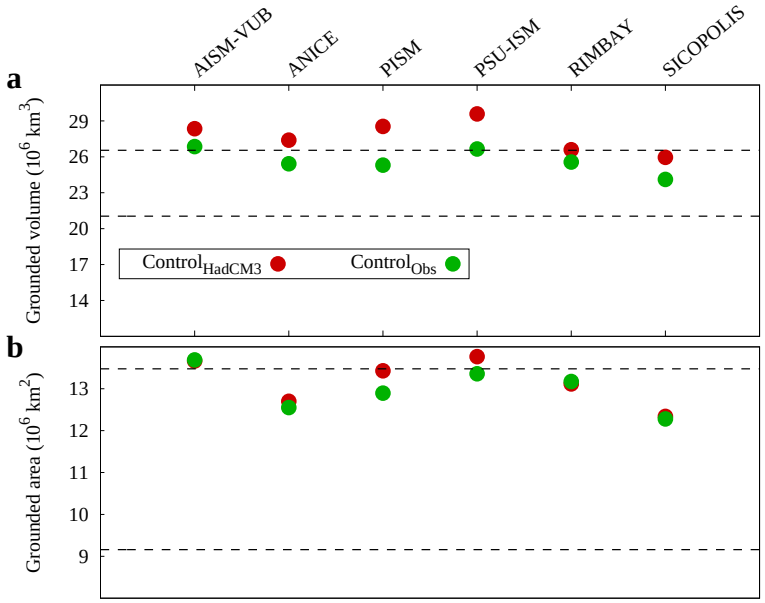

Figure 4. (a) Final grounded ice volume (10^6 km^3) and **(b)** final grounded ice area (10^6 km^2) for the control simulations. Control$_{HadCM3}$ in red, Control$_{Obs}$ in green. The horizontal dashed lines indicate the PD and Pliocene grounded ice volume and area of the initial ice-sheet topographies.

TCD
8, 5539–5588, 2014

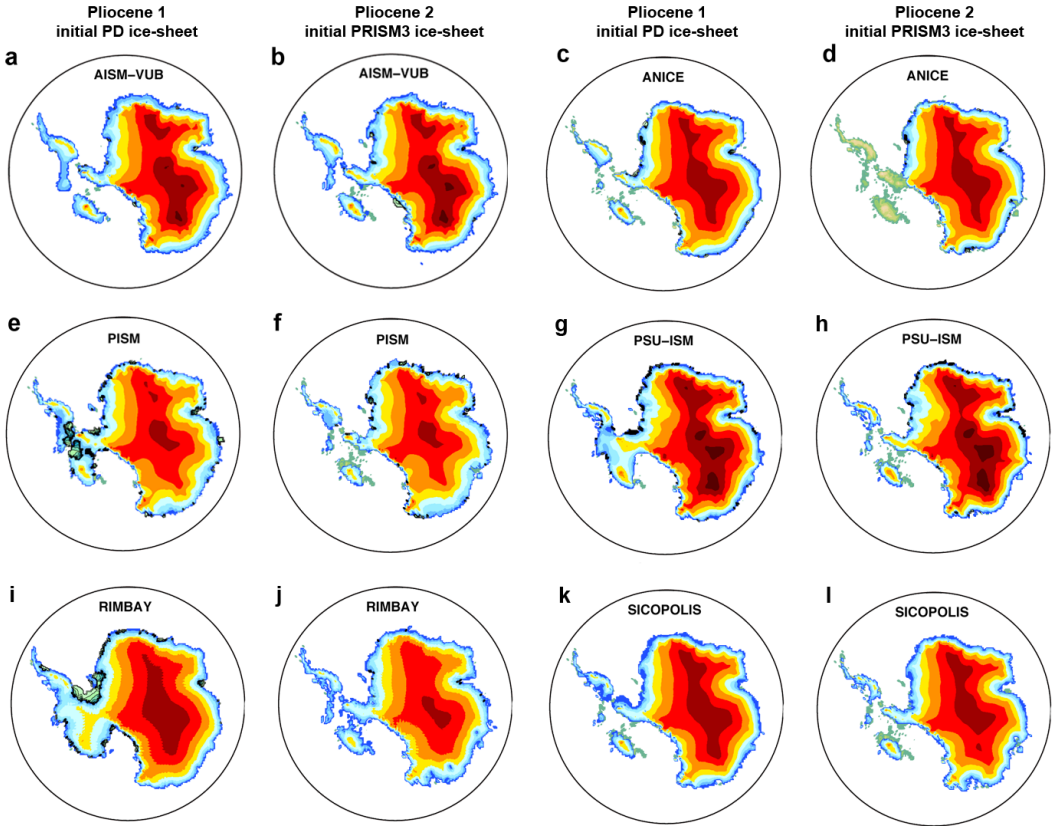

Figure 5. Ice surface topography and ice thickness of the ice shelves for the Pliocene simulations with HadCM3 Pliocene climate forcing. **(a)**, **(c)**, **(e)**, **(g)**, **(i)** and **(k)** show the final ISM topography for the Pliocene$_{\text{Ice-PD}}$ simulation with the initial PD ice sheet. **(b)**, **(d)**, **(f)**, **(h)**, **(j)** and **(l)** show the final ISM topography for the Pliocene$_{\text{Ice-PRISM3}}$ simulations with initial PRISM3 ice sheet. For all panels the colour scale is the same as in Fig. 3. **(a, b)** AISM-VUB, **(c, d)** ANICE, **(e, f)** PISM, **(g, h)** PSU-ISM, **(i, j)** RIMBAY and **(k, l)** SICOPOLIS.

TCD
8, 5539–5588, 2014

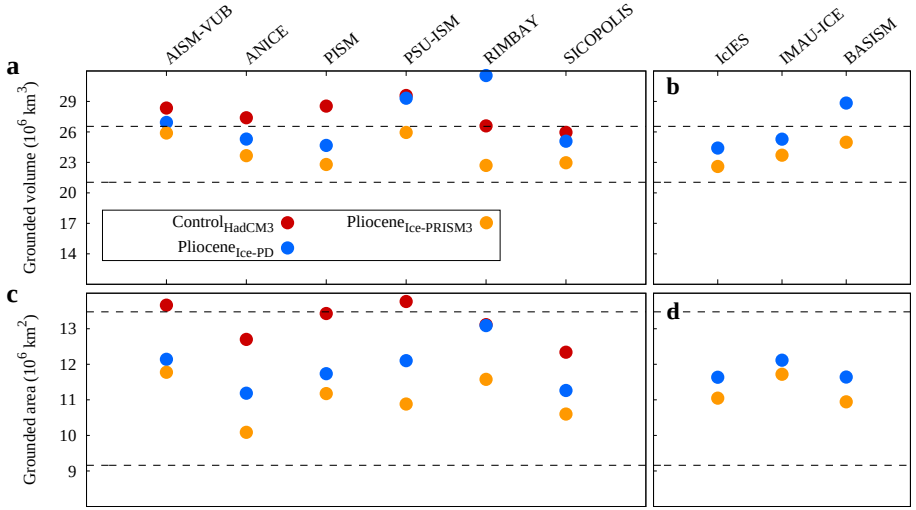

Figure 6. (a) Final grounded ice volume (10^6 km^3) for the SIA-SSA models and **(b)** for the SIA models. **(b)** Final grounded ice area (10^6 km^2) for the SIA-SSA models and **(d)** for the SIA models. Control$_{HadCm3}$ in red, Pliocene$_{Ice-PD}$ in blue and Pliocene$_{Ice-PRISM3}$ in orange. The horizontal dashed lines indicate the PD and Pliocene grounded ice volume and area of the initial ice-sheet topographies.

TCD
8, 5539–5588, 2014

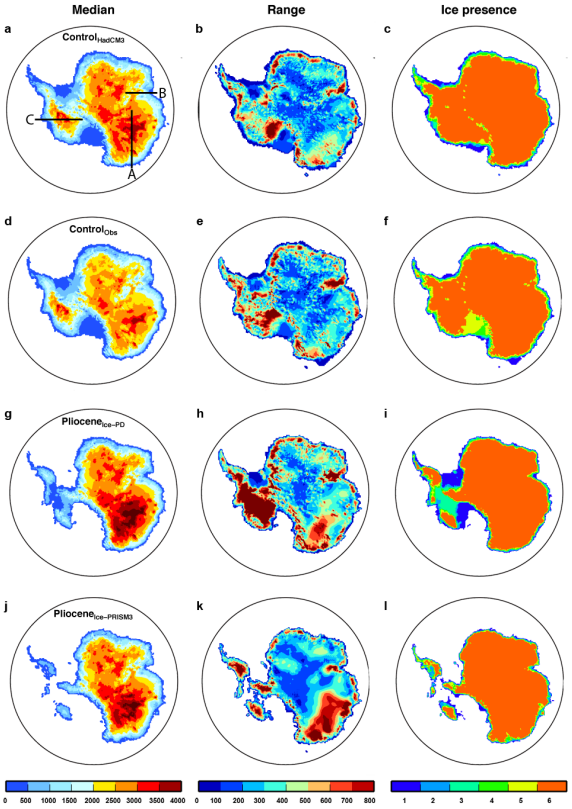

Figure 7. Median, range and coverages of ice thickness from the six ISM simulations. From top to bottom shows the four experiments. All six ice thickness values for each location are sorted, the median is shown as the mean of the 3th and 4th value (in m), the range is the difference between the 6th and the 1st, divided by two and ice coverage counts if any ice is present. The black lines in **(a)** represent the cross sections: A – Wilkes basin, B – Lambert ice stream and C – the WAIS.

TCD
8, 5539–5588, 2014

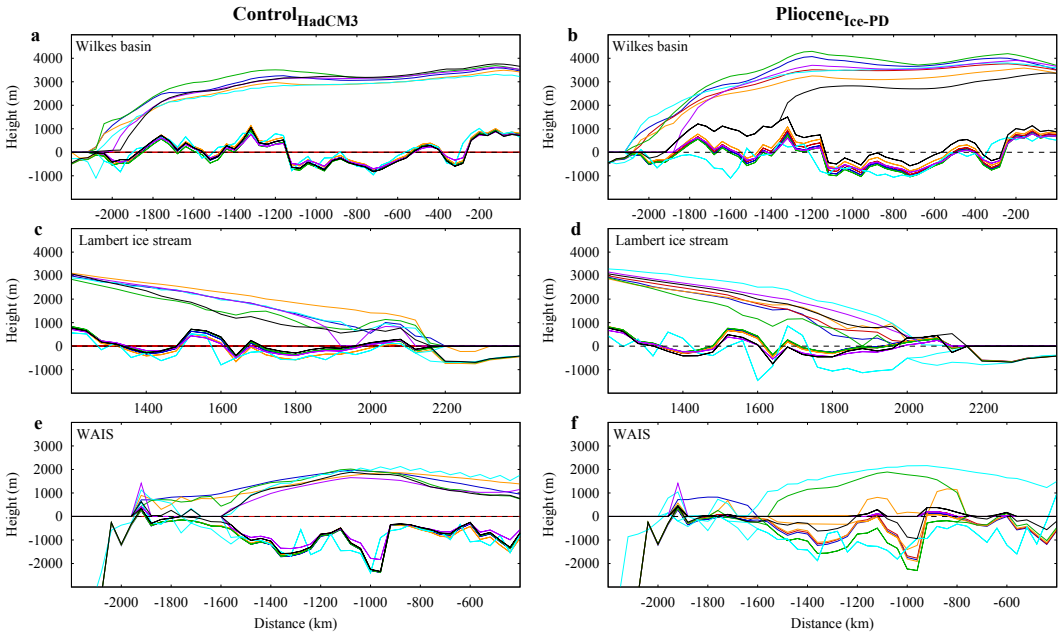

Figure 8. Cross section through the ice sheets showing surface and bedrock topographies. Cross sections as indicated in Fig. 7. Top row shows a cross section of the Wilkes basin, middle panels show the Lambert ice stream and bottom panels a cross section through the West Antarctic ice sheet. Left panels show the $Control_{HadCM3}$ simulation, the right panels for the $Pliocene_{Ice\text{-}PD}$ simulations. The colours represent the different models and match with the lines in Fig. 2, black lines indicate the PD topography **(a, c, e)** and the PRISM3 topography **(b, d, f)** of Bedmap1.

TCD
8, 5539–5588, 2014

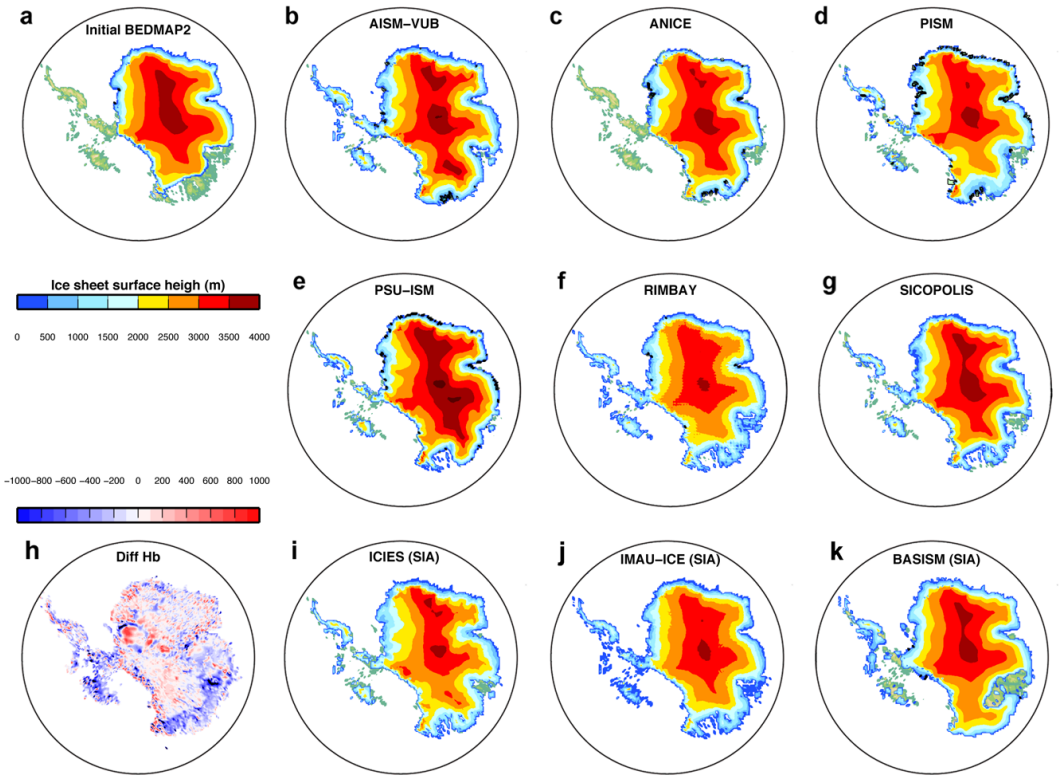

Figure 9. Ice surface topography and ice thickness of the ice shelves for the Pliocene$_{\text{Ice-PRISM3}}$ simulation with Bedmap2. **(a)** The initial PRISM3 ice sheet topography i s obtained by initialising the PRISM3 ice sheet on the Bedmap2 topography and let the bedrock rebound by using the ELRA model within ANICE. **(b)** AISM, **(c)** ANICE, **(d)** PISM, **(e)** PSU-ISM, **(f)** RIMBAY, **(g)** SICOPOLIS. **(h)** Difference between Bedmap2 and Bedmap1 bedrock topography for the PRISM3 initial ice sheet. SIA-only models; **(i)** IcIES, **(j)** IMAU-ICE, **(k)** BASISM.

TCD
8, 5539–5588, 2014

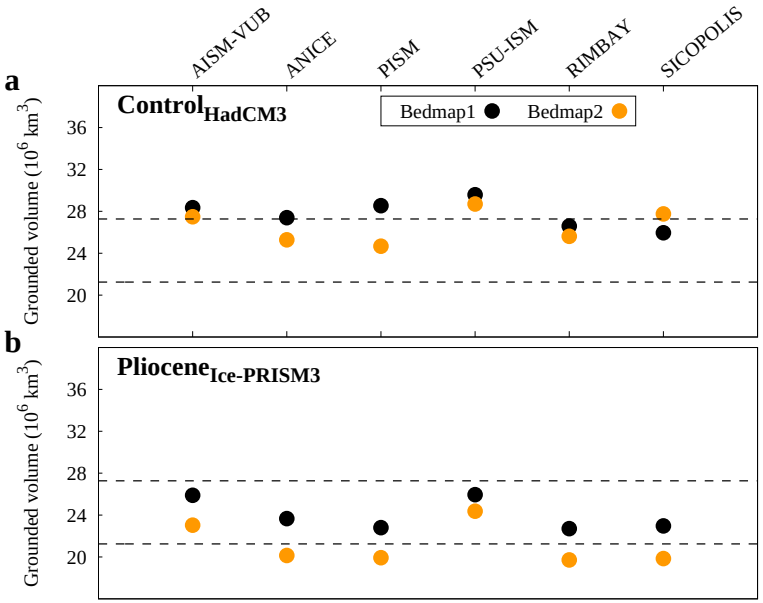

Figure 10. Final grounded ice volume (10^6 km^3) for the six models with the Bedmap1 (black) and Bedmap2 (orange) experiments. **(a)** for the $\text{Control}_{\text{HadCm3}}$ experiment and **(b)** for the $\text{Pliocene}_{\text{Ice-PRISM3}}$ experiment. The horizontal dashed lines indicate the PD and Pliocene grounded ice volume of the initial ice-sheet topographies with Bedmap2.

TCD
8, 5539–5588, 2014